IN SITU VOLUME STUDIES OF LI-ION POUCH CELLS

by

Julian Self

Submitted in partial fulfilment of the requirements
for the degree of Master of Science

at

Dalhousie University
Halifax, Nova Scotia
August 2015

I could be bounded in a nutshell and count myself a king of infinite space

—Hamlet

Table of Contents

List of Tables

List of Figures

Abstract

The lifetime of Li-ion cells can increase more than tenfold when a few weight percent of additives is added to the electrolyte of the cells. A principal challenge in understanding how these additives work is how they affect films formed on both the negative and positive electrodes.

Using Archimedes' principle, it is possible to measure the change in volume of flexible Li-ion pouch cells during charge and discharge by using equipment described in the present work. Quantitative knowledge of gases produced during the first charge, or "formation", of cells can allow insight into film-forming chemical pathways.

In this work, DFT (density functional theory) with a solvation model was used in the Gaussian quantum chemistry software package to further understand such pathways. The additives studied were prop-1-ene-1,3-sultone (PES) and vinylene carbonate (VC), where the control electrolyte was a mix of linear and cyclic carbonates with a conductive salt.

List of Abbreviations and Symbols Used

T_b	boiling point
C/t (or C-rate)	C/t : charge and/or discharge in t hours
Δm_{eff}	change in effective mass (measured weight divided by standard gravity g)
Δv	change in volume
ρ	density
DFT	density functional theory
ϵ	dielectric constant
DEC	diethyl carbonate
DEMS	differential electrochemical mass spectrometry
DMC	dimethyl carbonate
μ	dipole moment (in Debye, D)
EMC	ethyl methyl carbonate
EC	ethylene carbonate
FTIR	Fourier transform infrared spectroscopy
GTO	Gaussian-type orbitals
ΔG	Gibbs free energy change
$\Delta G\ddagger$	Gibbs free energy change for a transition state
k	Henry's constant in mol/(L atm)
k'	Henry's constant in MPa
HOMO	highest occupied molecular orbital
IEFPCM	integral equation formalism variant of the polarizable continuum model
IRC	irreversible capacity loss
M	transition metal(s) (in $LiMO_2$)
NMC	$Li[Ni_xMn_yCo_z]O_2$
LTO	$Li_4Ti_5O_{12}$
LCO	$LiCoO_2$
LIB	Li-ion battery
LCAO	linear combination of atomic orbitals
LiBOB	lithium bis(oxalate)borate
LBDC	lithium butylene dicarbonate
LEC	lithium ethyl carbonate
LEDC	lithium ethylene dicarbonate
LMC	lithium methyl carbonate
LUMO	lowest unoccupied molecular orbital
MS	mass spectrometer
MAGE	measuring Archimedes' gas expansion

T_m	melting point
n_s	moles of dissolved gas
n_g	moles of gas in gas phase
NIST	National Institute of Standards and Technology
NMR	nuclear magnetic resonance
OEMS	online electrochemical mass spectrometry
P_x	partial pressure
PEC	polymeric ethylene carbonate
PK	polyketone
P	pressure
PES	prop-1-ene-1,3-sultone
PC	propylene carbonate
Rad	radical
RT	room temperature (298.15 K)
SIM	single ion monitoring mode (SIM)
SEI	solid electrolyte interphase
E^0	standard reduction potential
n_t	total number of moles of gas
TS	transition state
TEM	transmission electron microscopy
VC	vinylene carbonate
η	dynamic viscosity
V	Volt(s)
v_g	volume of gas in gas phase
v_s	volume of liquid electrolyte into which gas is dissolved
wt %	weight fraction (in percent)
XPS	X-ray photoelectron spectroscopy

Acknowledgements

Chapter 1: Introduction

In both public and private sectors, improving the lifetime and lowering the monetary cost of Li-ion batteries (LIB) is being sought after arduously.[1] LIB applications include electric vehicles and grid energy storage. One way to increase the lifetime of a Li-ion cell by over tenfold is to add to standard electrolyte solutions certain chemical compounds on the order of a percent fraction of the weight.[2] These compounds are called electrolyte "additives". The present work seeks to further understand the role that two additives play, namely vinylene carbonate (VC) and prop-1-ene-1,3-sultone (PES). This chapter is devoted to introducing the basic operation of a Li-ion cell, motivation behind picking the composition of typical solvent blends, the solid electrolyte interphase (SEI) on the negative electrode and the positive electrode/electrolyte interphase.

1.1 LIB Operation

A set of electrochemical cells to store energy can be referred to as a battery of cells, or simply a battery.[3] Rechargeable batteries are also called secondary batteries, a subset of which are Li-ion batteries. These move lithium ions (Li^+) through a conductive electrolyte solution from electrode to electrode during charge and discharge.[3] Figure 1.1 shows schematic the charging process of a Li-ion cell where Li-ions intercalate in the graphitic negative electrode during charge after having moved through an electrolyte. During charge, electrons must move in the direction of the arrows in Figure 1.1, which can be done by
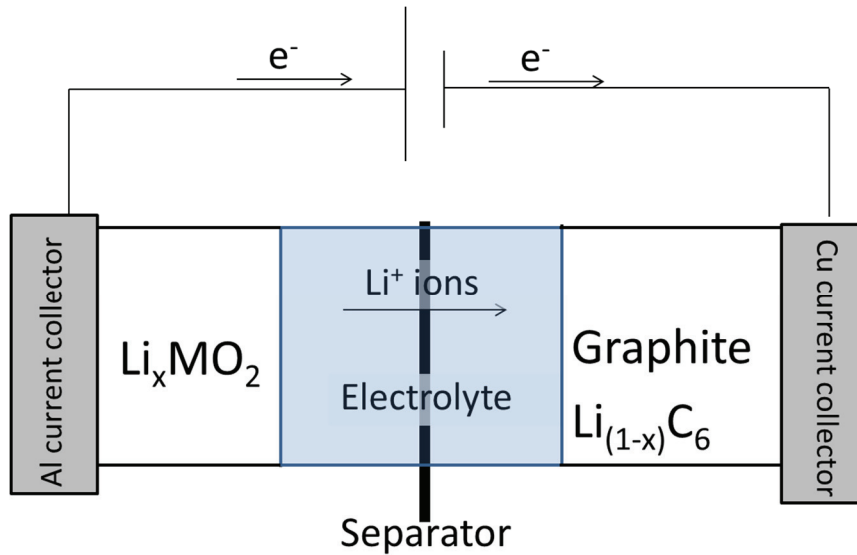
Figure 1.1: Schematic of a Li-ion cell during charge where Li-ions move from the positive LiMO$_2$ electrode into the graphitic negative electrode.[3] Each intercalation of a Li-ion is accompanied by an e$^-$ provided to the electrode, as shown by the direction of the arrows. Al and Cu current collectors are shown attached to their respective electrodes.

providing a current to the cell. Each intercalation of a Li-ion into an electrode is accompanied by an e$^-$ being provided to the electrode. The reverse process occurs for discharge, which can provide power to the external circuit. A separator placed between the electrodes prevents an internal short but allows the flow of Li-ions. The positive electrode can be LiMO$_2$ where M is a mix of transition metals. For example, both M = Co (LCO) and M = Ni$_x$Mn$_y$Co$_z$ (NMC, where x+y+z = 1 and xyz ≠ 0) are popular positive electrodes.[3] The negative electrode can be a variety of materials, e.g. graphite, silicon, etc.[3-5]

1.2 Li-ion Battery Electrolyte

Water cannot be easily employed as an electrolyte solvent in Li-ion cells due to its strong reactivity with lithiated graphite. Li-ion cells use nonaqueous electrolyte solutions.[6] Aurbach divides nonaqueous electrolytes into five groups: organic and inorganic solvents in liquid solutions, molten salt liquid systems, conducting polymers (ionically and/or electronically), liquefied gas based solutions and ionically conducting solids such as doped oxides.[6] Here, only a small subset of the former group will be considered: liquid solutions based on organic carbonates.

Xu lists five main criteria for a good electrolyte solution:[4]
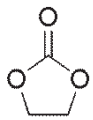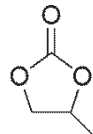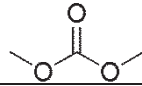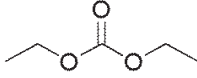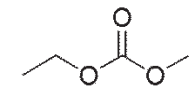
1) ability to dissolve salt, or equivalently, a high dielectric constant, ε;

2) low viscosity, η, for ion transport;

3) inert to cell components both in charged or discharged states of the Li-ion cell;

4) low melting point, T_m, and high boiling point T_b;

5) and safe, or equivalently, non-toxic and non-flammable.

No single electrolyte solvent is optimal for all criteria, but some mixtures are significantly better than others. One approach to electrolyte design is to pick co-solvents that can, together, remedy the shortcomings of their partner co-solvent(s). To fulfill criteria 1), cyclic solvents containing, for example, carbonyl (C=O) or sulfonyl (S=O) groups can be considered due to their high polarity and dielectric constant. However, alone, these may be too viscous, thus a mixture with a linear carbonate may allow both a reasonably high ε and low η. Table 1.1 shows the relevant properties for two cyclic carbonates, EC (ethylene

carbonate) and PC (propylene carbonate) as well as three linear carbonates, DMC (dimethyl carbonate), DEC (diethyl carbonate) and EMC (ethyl methyl carbonate).[4] These five carbonates are by no means the only solvent components worth considering, although these are perhaps some of the most widely employed in consumer electronics. When two or more of these solvents are mixed, the resulting values of T_m, T_b, ε or η of the mixtures are somewhere in between the values of the individual solvents.[6–8] Thus, mixing a cyclic and linear carbonate can allow both a reasonably high dielectric constant and low viscosity. For the linear carbonates, DMC, DEC and EMC, there is a trade-off between large operating temperature window and low η. Although PC-containing solutions may perform better at low temperatures than EC, PC may lead to a more pronounced destruction of the graphite negative electrode.[4]

Although many conductive salts can be considered, $LiPF_6$ is the most popular because it has a sufficient conductivity, ionic mobility and dissociation constant.[4,8] Based on conductivity measurements, 1 M of $LiPF_6$ was found to be optimal in solvent blends of EC:EMC 3:7.[8] This is the electrolyte solution taken as the "control" electrolyte throughout the rest of the present work. Although the 3:7 ratio may seem arbitrary, there is a trade-off between having a low T_m, low η and high enough ε for the binary mixtures. Other mixtures may be suitable but are outside the scope of this work. Other salts, such as $LiBF_4$ or LiBOB (lithium bis(oxalate)borate), are also currently used in electrolyte solutions.[4,5]

Table 1.1: Common electrolyte co-solvents with their reported melting point T_m, boiling point T_b, dielectric constant ε and viscosity η.[4,9]

Solvent	Chemical structure	T_m/T_b (°C)	ε at RT	η (mPa·s at RT)
EC		36/248	90	1.90 (40 °C)
PC		-49/242	65	2.53
DMC		5/91	3.1	0.59 (20 °C)
DEC		-74/126	2.8	0.75
EMC		-53/110	3.0	0.65

1.3 Solid Electrolyte Interphase at the Graphite Negative Electrode

Although suggested as a desirable quality in Section 1.1, electrolyte components are never completely inert to electrode materials. Generally, during the first charge, electrolyte components are initially decomposed or reduced to form a passivation layer on the negative electrode, after which the reactions are suppressed by larger kinetic barriers. Ideally, this involves formation of a layer that allows transport of Li-ions but prevents electron transfer.

Reportedly, Peled was the first to suggest the idea of a so-called solid electrolyte interphase (SEI).[4] Although first suggested for Li-metal negative electrodes, it was later adapted for carbonaceous negative electrodes.[10] Peled et al. argue that an initial, mostly inorganic film is first formed, which is followed by formation of a mostly organic film. Figure 1.2 shows a cartoon SEI where an inorganic layer is closer to the graphite negative electrode while an outer organic layer is closer to the electrolyte. Peled et al. suggest that the inner inorganic film may include species such Li_2O, LiF or Li_2CO_3.[11] The outer organic film may include polyolefins or semicarbonates.

Understanding the exact nature of a given SEI is a principal challenge in the LIB research community. Since the SEI contains chemical species involving Li-ions, the first cell charge, during which the SEI is initially formed, is accompanied by a considerable irreversible capacity loss (IRC).[3] The SEI, through its evolution or growth, may also lead to cell failure, impedance rise and further loss of capacity during both storage and cycling.[2] Electrolyte additives[4,5] may modify the SEI, which can increase the cycle life of cells by an order of magnitude.[2] A more accurate representation of graphitic negative electrode SEI can be found in the review by Verma et al., where spectroscopic results, namely from FTIR (Fourier transform infrared spectroscopy) and XPS, are compiled to give a detailed list of SEI components.[12]
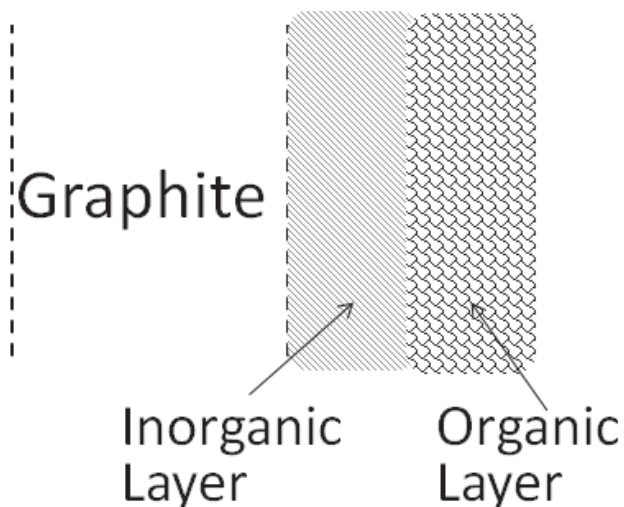
Figure 1.2: SEI cartoon schematic where the graphite negative electrode is covered by an organic layer stacked over an inorganic layer.

Lithium ethylene dicarbonate (LEDC) has been suggested as the main reduction product from EC. Zhuang et al. synthesized LEDC and compared its FTIR spectrum to cells with EC:EMC 3:7 w/ 1.2 M LiPF$_6$ subjected to cyclic voltammetry. They found LEDC to be the dominant film species on a Ni electrode.[13] This is consistent with results from Nie et al. who found strong evidence for LEDC as a dominant SEI component on the graphite negative electrode with EC-based control electrolyte, using XPS and nuclear magnetic resonance (NMR) measurements.[14]

Perhaps the most detailed proposed pathway for LEDC formation was suggested by Wang et al. in their 2001 density functional theory (DFT) study of ethylene carbonate reduction. This pathway is shown in Figure 1.3a, where an EC-radical (EC-Rad),

originating from reduction and lithium coordination of EC, can dimerize to form either LEDC or lithium butylene dicarbonate (LBDC). In their publication, the authors state:

"[EC-Rad's] Gibbs free energy of reaction (ΔG = -67.4 kcal/mol) is the most favorable among the involved reactions. Nucleophilicly [sic] attacking the radical center by oxygen, [EC-Rad] could undergo another dimerization probably without barrier (transition state has not been found, [for LEDC formation]), bringing about lithium ethylene dicarbonate, $(CH_2OCO_2Li)_2$ [LEDC], which is the most common product found experimentally."[15]

The "radical center by oxygen" is an ill-defined phrase, but perhaps Wang et al. intended to imply instead "attacking the radical center with oxygen". Anyhow, a possible LEDC formation pathway from EC-Rad dimerization is shown by the arrow-pushing mechanism illustrated in Figure 1.3b, which may be what Wang et al. intended to imply. Another, similar, but perhaps even more confusing scheme appeared years prior in Aurbach et al.'s 1999 paper, where an LEDC formation scheme was illustrated with an implication of surface mediation, which Aurbach et al. call disproportionation.[16] The author of the present work tried to clarify this scheme through its illustration in Figure 1c. Aurbach et al. also suggest the alternative pathway: "or by a two-electron transfer which form[s] CO_3^{-2}, which further attacks nucleophilically another molecule of EC."[16,17] the
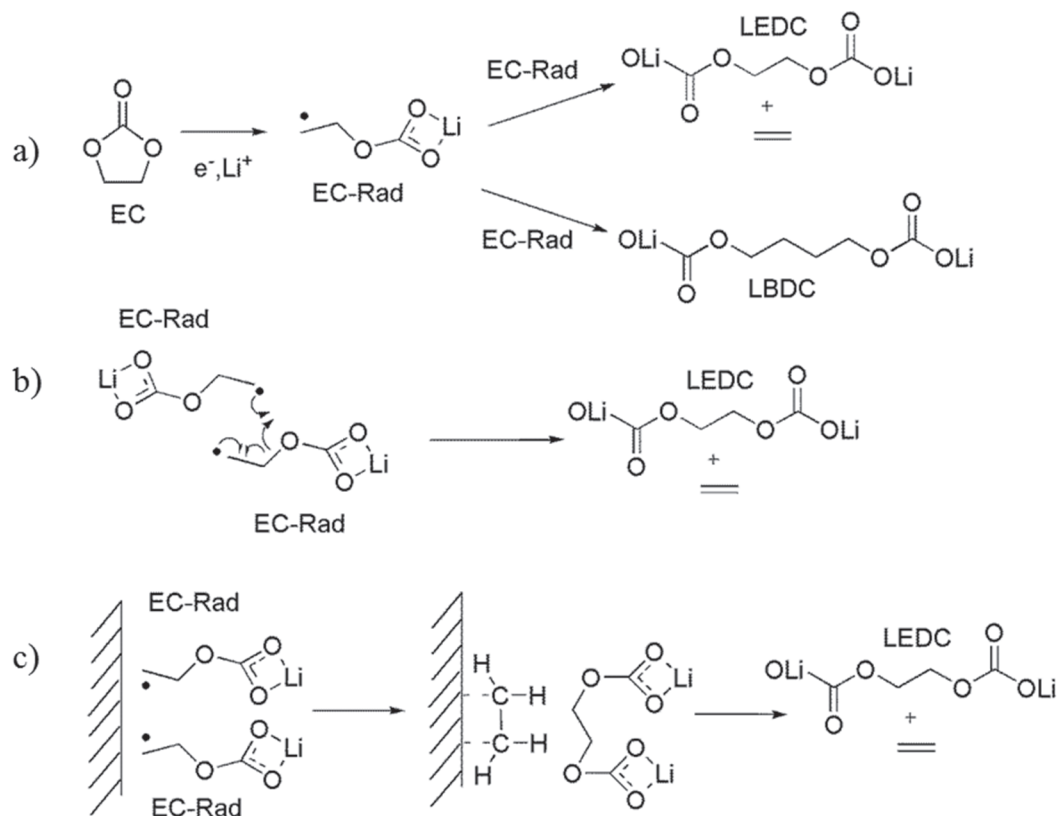
Figure 1.3: a) EC reduction into the radical EC-Rad, which can dimerize into LEDC with C_2H_4 and LBDC, as suggested by Wang et al.[15] b) The author's interpretation of the mechanism of Wang's et al. in a). c) The surface mediated suggestion by Aurbach for LEDC formation.[16]

ratio of LEDC to LBDC in EC reduction processes remains ambiguous. Zhuang et al. concluded that the absence of LBDC in their FTIR measurements may be due to solubility of the species.[13]

It has been also argued that EC can be twice reduced into Li_2CO_3 and C_2H_4,[15,18] as illustrated in Figure 1.4. Xu speculates that, after the SEI is initially passivated, in part by

the Li_2CO_3 species, EC would only be singly reduced, e.g. into LEDC and C_2H_4, due to the poorer electronic conductivity of the initial, perhaps mostly inorganic, passivation film compared to the pristine graphite surface.[4] This would be consistent with the schematic shown in Figure 1.2.
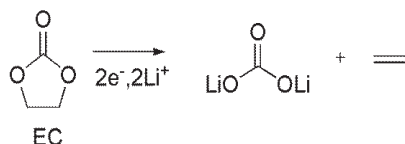
Figure 1.4: Double reduction of EC into Li_2CO_3 and C_2H_4.

Although the linear carbonate co-solvent EMC can react with lithiated graphite to form lithium ethyl carbonate (LEC) and lithium methyl carbonate (LMC),[14] its reactivity is suppressed once used with the co-solvent EC due to the much lower dipole moment of linear carbonates compared to cyclic carbonates.[6] Thus the reduction of EC largely defines the negative electrode SEI, which has been found by transmission electron microscopy (TEM) to be on the order of 10 or sometimes 100 nm thick.[14]

1.4 Positive Electrode/Electrolyte Interphase

The interphase formed at the positive electrode of Li-ion cells, sometimes called SEI,[5] is less understood then the negative electrode SEI, and has also been subject to less investigation. One chemical species often found on Li-ion positive electrodes is Li_2CO_3, which may have accumulated on the surface of the positive electrode during manufacturing processes. Upon contact with atmosphere or the electrolyte salt, species of Li_2O or LiF may also form.[5] Preferential adsorption of the polar EC co-solvent over its linear carbonate co-

solvent has been suggested.[5] Subsequently, formation of a polymeric ethylene carbonate species (PEC) has been suggested by Yang et al., whose FTIR and XPS measurements provide evidence for PEC,[19] which is shown in Figure 1.5. The
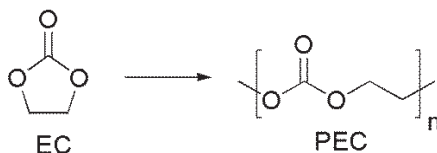
Figure 1.5: Illustration of polymeric ethylene carbonate (PEC), for which there is evidence at the positive electrode.[19]

degradation of PEC at high cell voltage (e.g. ~4.7 V at the positive electrode) has been suggested to result in formation of a new polymer after release of CO_2.[5] Notably, at high voltage, electrolyte and/or film degradation at the positive electrode is often referred to as electrolyte oxidation, despite the ambiguity as to the exact chemical pathways or mechanisms occurring during the degradation.[5]

1.5 Outline of Thesis

In Chapter 2, the MAGE (Measuring Archimedes' Gas Expansion) device is described. This device allows in situ volume measurements of Li-ion pouch cells, i.e. volume change as function of both time and cell voltage. This can indicate whether gaseous reactions in a cell will lead to failure (inoperability). Also, combined with other tools, such measurements can provide insight into certain of the important chemical reactions occurring in the cell. These volume measurement methods can not only be applied to study the additives VC and PES but general electrolyte blends with varying

positive or negative electrodes. For a control electrolyte, as well as control + 2 wt % VC and control + 2 wt % PES, collected in situ volume data and relevant gas-chromatography mass-spectrometry (GC-MS) results are presented.

Chapter 3 is devoted to mapping out the gas-producing pathways of cells with the PES additive. The quantum chemistry package Gaussian is used with DFT and the IEFPCM solvation model. The solid by-products of the proposed gaseous reactions do not explain all relevant X-ray photoelectron spectroscopy (XPS) data. Thus, pathways of reduced PES reacting with solvent components are considered. These allow suggestion of "building block" components of the film formed on the negative electrode.

Chapter 4 focuses on assessing the plausibility of a widely suggested theory involving the precise chemical role of VC: its chain growth through monomer addition, also known as oligomerization. The co-oligomerization of ethylene is also studied. For the positive electrode, protonated VC as an initiator is considered for the formation of the oligomer. Finally, decarboxylation of the oligomer is proposed, and may explain the relationship between CO_2 production and VC. Chapter 5 outlines potential experiments and further scientific work to continue investigation into VC, PES and other additives for Li-ion cells.

Chapter 2: Volume Measurements

In 2013, the British newspaper Guardian reported that "Samsung is offering a trade-in program on batteries for its flagship Galaxy S4 smartphone after some users complained they were draining rapidly or even swelling."[20] Evidently, the LIB used in the Galaxy S4 electronic device had produced so much gas during its operation that it was unusable. Gas creation is a serious concern for the operation of Li-ion cells. Large amounts of gas can completely deform and expand a Li-ion pouch cell, and it may take more room than can fit in its host device. Gas creation can even mechanically destroy cells. For example, the increase in pressure from excess gas can modify an electrode stack and negatively affect Li-ion diffusion.

It is well known that as Li-ions intercalate into the negative electrode during charge, the volume of the negative electrode reversibly increases.[21,22] However, such expansion is typically systematic, predictable and can be accounted for. Often, gas production can lead to a much more considerable volume increase than the volume expansion during charge due strictly to intercalation.[23] Berkes et al. note that "processes that cannot be perceived unambiguously from purely electrochemical data include dissolution/loss of active material components, fading of certain electrode regions, and reactions that occur in the electrolyte phase, such as decomposition and gas evolution."[24] All of these reactions can be detrimental to cell cycle-life, and thus knowing when and how such individual processes take place is of practical significance. This chapter will focus on measurement techniques for one of these specific reactions, namely gas evolution.

Gas reactions are not always strictly deleterious as they can come about as products

of SEI-forming mechanisms. For example, the formation of the important SEI component LEDC, as introduced in Chapter 1, is accompanied by formation of ethene (C_2H_4). And so, if the gaseous reactions can be understood, it is likely that certain film-forming mechanisms on both the negative and positive electrodes can be better understood.

2.1 Volume Measurement Techniques

In 2013, Li et al. reported using a simple technique to measure volume change. They measured the thickness of pouch-cells with a Vernier caliper.[25] This allowed them to loosely determine whether the studied electrolyte additive led to more or less gas formation. The obvious drawback of this method is the lack of accuracy. For example, it is ambiguous where along the pouch cell the thickness should be measured, and to what extent such measurements are repeatable.

Another reported ex-situ (static) type of measurement involves using Archimedes' principle, which states that the buoyant force of a submerged object is equal to the weight of the displaced fluid. The volume of the displaced fluid in this case is equal to the volume of the submerged object. If the change in effective mass Δm_{eff} of such a submerged object is measured with a balance, it can be derived that

$$(2.1) \quad \Delta v = -\Delta m_{eff}/\rho$$

where Δv is the change in volume of the submerged object and ρ is the density of the fluid into which the object is submerged.[23] Wang et al. used Archimedes' principle to study the change in volume of pouch cells after certain cycling protocols.[26] The cells were submerged in de-ionized water and were attached under a balance using a fine wire hook.

14

This allowed determination of Δm_{eff} and thus Δv, using equation 2.1, for cells before and after certain charging protocols, with a given electrolyte mixture.

Gas evolution can also be measured in situ. In other words, gas evolution is probed while a cell is being charged or discharged. Hartmann et al. reported using in situ pressure measurements of a rigid can cell for metal-air batteries.[27] In this case, the volume of gas was fixed due to the rigidity of the cell's casing. And so, an increase in pressure allowed inference of an increase in moles of gas. An even more elaborate setup is required for the in situ probing of gas using online electrochemical mass spectrometry (OEMS),[24] sometimes also called differential electrochemical mass spectrometry (DEMS).[28] OEMS measurements typically use a combination of either a flow meter[28–30] or pressure sensor[24,31] with a mass spectrometer (MS) which allows determination of gas production as a function of time and cell voltage for a given operating temperature. Such measurements do not only provide an estimate of the amount of gas produced, but also of the nature of the gas produced, due to the MS detection.

2.2 MAGE Setup

In order to obtain in situ volume change measurements for Li-ion pouch cells, the setup involving Archimedes' principle described previously can be further adapted following the work of Aiken et al.[23] Provided a submerged cell can be charged or discharged while having its weight measured, dynamic measurements can be obtained. A detailed account of such an implementation, called MAGE, is herein described.

2.2.1 Temperature-controlled Box

In order to conduct different sets of experiments at given fixed temperatures, temperature-controlled boxes were designed. These followed closely the design as described by Dahn et al.[32] Briefly, there is an inner metal box around which a band heater is wrapped. Silica insulation is then also used around the metal box and heater, and finally these components are all enclosed in an outer metal box. The latch-controlled door uses silica insulation as well. A temperature controller is used with the band heater, which allows temperatures from 25.0℃ to 70.0℃ with an error of ±0.1℃. The experiments are sensitive to external vibration and so the boxes are placed on vibration-cancelling ceramic slabs so that nearby footsteps and do not affect the data, although the boxes are still sensitive to the touch.

2.2.2 Single Stand Components

Inside each temperature-controlled box are 6 stands that hold the necessary components for in situ measurements of one pouch cell. Figure 2.1 shows one such stand with the different parts labelled. For this specific design, the pouch cell has a starting volume on the order of 2 mL and a capacity on the order of 200 mAh. The Li-ion cell hangs from a steel hook which, in turn, hangs from a thin film load cell. This 0.2 N load cell (from the SMD company) produces an output voltage directly proportional to the weight hanging from it. A detailed description of the strain gauge can be found in Aiken et al., who have an almost identical setup.[23] Notably, the set up for the present work expanded on theirs by building more available channels. Mechanical pump oil was used as it has low vapour

pressure and is non-conductive. Terminal blocks were attached to the cell tabs with soldered 70 μm diameter copper wires. The wires provided for both voltage measurements and current provision to the Li-ion cell. These enameled wires were purchased from TEMCo (Soderon RED Wound, Copper magnet wire 45 GA).
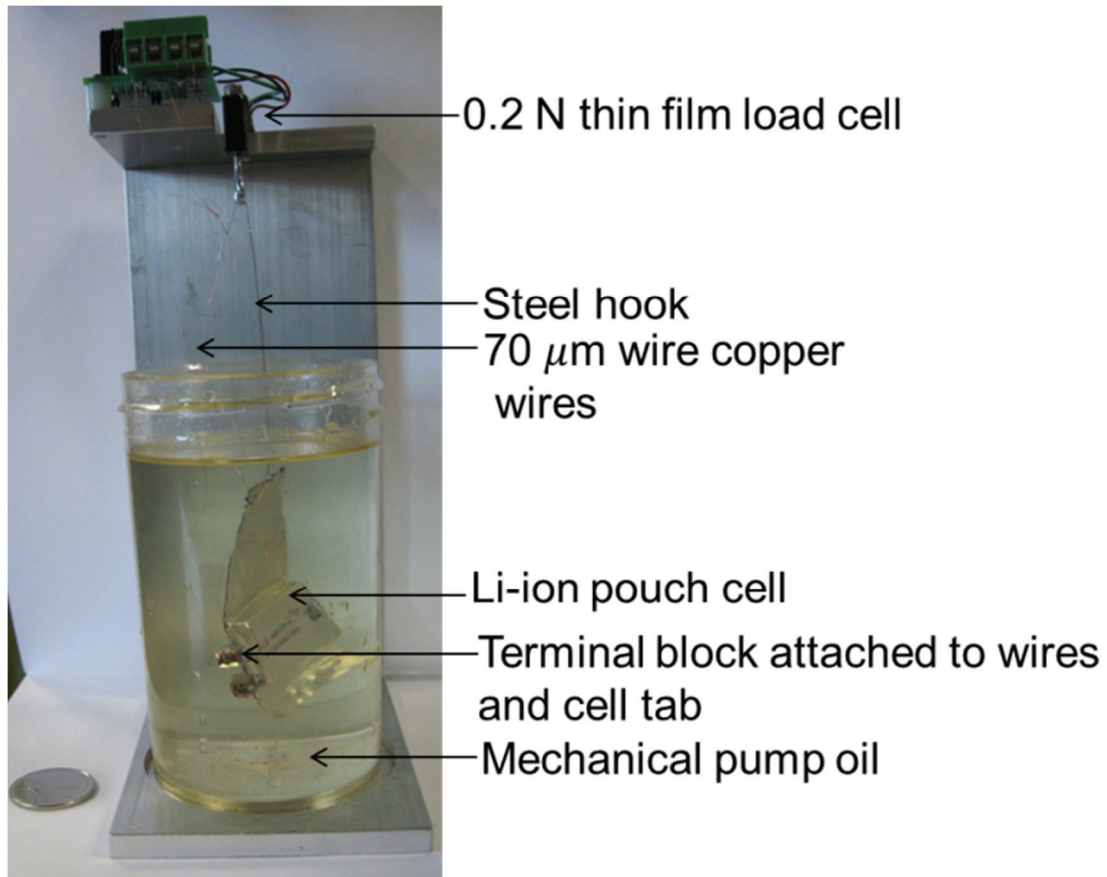
Figure 2.1: Picture of a MAGE (Measuring Archimedes' Gas Expansion) stand

2.2.3 Interface and Data Acquisition

Figure 2.2 shows a schematic of the devices used for a given stand in the MAGE apparatus. A proper circuit diagram of a similar setup can be found in Aiken et al.[23] The

strain gauge requires a given voltage for functionality (10 V), and so the necessary current is provided by a power source (Keithley SourceMeter 2401). The cell in the stand is charged by a computer controlled cell charger (Neware BTS3000). The cell charger also measures the voltage across the cell, which is relayed back to the computer. The multimeter (Keithley 2700) allows measurement of the strain gauge voltage and cell
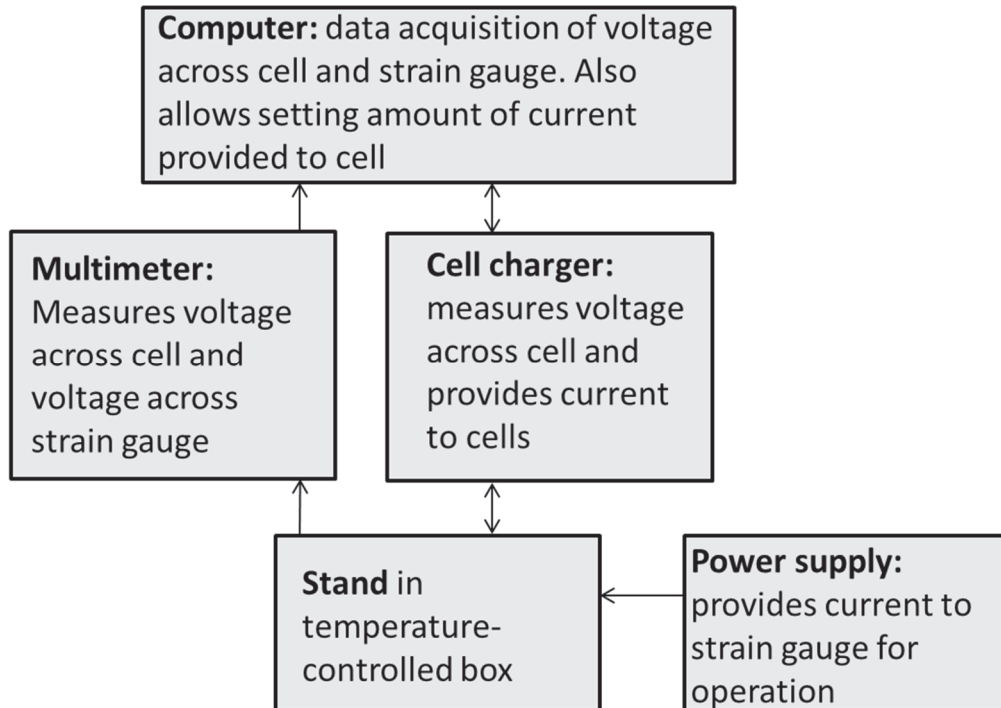
Figure 2.2: Schematic of devices used around a MAGE stand. The direction of the arrows indicates flow of information or current.

voltage as well, both which are relayed to the computer through a GPIB (General Purpose Interface Bus) interface. The stand connects to the multimeter, cell charger and power source via the 8 wires in an ethernet cable which is simply used as a convenient cable.

18

In-house software was designed to collect the strain gauge and cell voltage measurements as a function of time. The strain gauges had to first be calibrated, which was done using 6 masses of different weights between 0.4 g and 6.0 g. For each strain gauge calibration, the R^2 correlation coefficient of the linear fit was always above 0.999. Thus, the scatter about the calibration fit is negligible compared to the error from the measured weight of the different calibration masses, which is ±0.0002 g.

For every outputted strain gauge voltage, the software took a flat (non-weighted) average of 15 data points, sampled over 150 s (1 data points every 10 seconds) for a given strain gauge. This allowed independent, averaged strain gauge voltage measurements to be the final output for sampling intervals typically of 3 minutes, and never more than 10 minutes. These allowed computation of the change in volume using equation 2.1 where the measured density of the hydrocarbon oil $\rho = 0.840 \frac{g}{mL}$ (from 25°C to 70°C measured with a balance and a 100 mL volumetric flask). Thus, the final output provided for a given time includes not only the strain gauge voltage, but the change in volume and the voltage across the cell. Figure 2.3 shows data acquired with the MAGE system for a 245 mAh pouch cells (v ~ 2 mL) left on open circuit (further details on cell preparation can be found in the following subsection). Here, the random noise is on the order of 0.005 mL (or 5 μL), agreeing with the noise levels from an almost identical setup constructed by Aiken et al.[23]
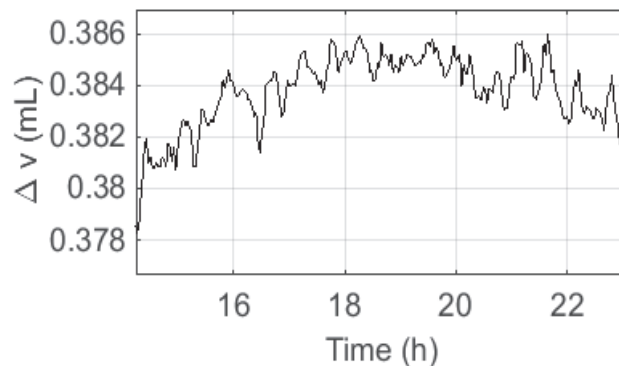
Figure 2.3: Change in volume as a function of time for a sealed pouch cell left on open circuit in a MAGE device.

2.3 Survey of Gas Expansion in Li-ion Pouch Cells

(Some parts of the following subsection are taken directly from Self et al.[33])

As explained in Chapter 1, the electrolyte in Li-ion cells reacts with both the negative and positive electrodes during the very first charge of the cells,[16,18,34,35] which is called often called "formation". In addition, further reactions occur as cells are continuously operated and the rates of these reactions generally increase with temperature.[36–38] Products of these reactions are solids, liquids and/or gases.[18,36] It is difficult to probe the solid and liquid reaction products in situ in commercial Li-ion cells but the volume of gas phases produced can be easily probed in situ using the MAGE setup. A previously unreported but significant feature, gas consumption, is also revealed by the measurements. Two additives are studied, namely VC (vinylene carbonate) and PES (prop-1-ene-1,3-sultone). Motivation for choosing the additives PES and VC will be provided in detail in Chapters 3 and 4, respectively.

20

Figures 1.3 and 1.4 in Chapter 1 showed reduction pathways for EC. Although no adequate quantitative model has been presented with regards to such mechanisms, there have been detailed theoretical (DFT) studies of both EC and VC reduction pathways, where produced gases include ethene (C_2H_4) and ethyne (C_2H_2).[15,39] Gas creation at the positive electrode and gas consumption occur through other mechanisms. It has been argued, both experimentally and through computation work, that EC can be oxidized to produce mainly CO_2, and CO in much smaller quantities.[40–42] Gas consumption has, to the authors' knowledge, however not been the subject of much scholarship, however, as will be shown, occurs and is important. There nonetheless have been suggestions that gases could polymerize on the surface of electrodes, e.g. ethene could polymerize into polyethylene on a graphite negative electrode,[16] or ethyne could form polyacetylene on the negative electrode due to its high reactivity.[43]

By studying the change in volume of cells during the first charge, this work introduces three important features in terms of volume change: a first gas step, at low voltage, gas consumption, and a second gas step at higher voltage. Gas chromatography-mass spectrometry (GC-MS) was used to identify gaseous species other than H_2 in cells using control, VC and PES electrolyte.

2.3.2 Experimental

The pouch cells employed in this study were all $Li[Ni_{0.4}Mn_{0.4}Co_{0.2}]O_2$ (NMC442)/graphite cells with a capacity of 245 mAh balanced for 4.7 V operation. The cells were produced by Li-Fun Technology (Xinma Industry Zone, Golden Dragon Road,

Tianyuan District, Zhuzhou City, Hunan Province PRC, 412000). All pouch cells were vacuum sealed without electrolyte in China and then shipped to our laboratory in Canada. Before electrolyte filling, the cells were cut just below the heat seal and dried at 80℃ under vacuum for 12 h to remove any residual water. Then, the cells were transferred immediately to an argon-filled glove box for filling and vacuum sealing. The NMC/graphite pouch cells were filled with 0.9 g of electrolyte. After filling, cells were vacuum-sealed with a compact vacuum sealer (MSK-115A, MTI Corp.). The electrolyte used had 1M of $LiPF_6$ (99.97% pure, BASF) in EC:EMC 3:7 (by volume, BASF, water content < 20.0 ppm) for the "control" electrolyte. For the studies involving additives, VC (BASF, 99.97%), PES (Lianchuang Medicinal Chemistry Co., Ltd., China, 98.20%) were used. The percentage of additive refers to the percentage by weight (e.g. 2% VC is 2 wt % of the electrolyte mixture). Before charging, all cells were held at 1.5 V for 24 h to ensure excellent wetting of the electrolyte in the jelly roll of the pouch cell.

Although the random error in the strain gauge measurements, due to the resolution, has been measured to be 5 μL, the systematic error from duplicate measurements of pouch cell gas evolution is much larger. The latter is judged to be 0.1 mL. This value was estimated from duplicate measurements, as shown in Figures 2.4 and 2.6.

For certain cells, GC-MS was used to analyze the different gases other than H_2 present at either 3.7 V or 4.7 V. Prior to GC-MS analysis, cells were charged on a Neware battery cycler in a 40.0 ± 0.1°C temperature box at current density of C/10. After reaching the set potential cells were immediately removed from the temperature box and put in a

brass chamber. The chamber was fitted with a swage lock quick connect on one end, and a septum on the other end. The cap of the chamber was fitted with a shaft, having a sharp point, allowing the pouch cell bag to be punctured. The shaft was fitted with two o-rings to prevent gas exchange between the exterior and the interior of the chamber.

The brass chamber with the cell fitted inside was pumped down to an absolute pressure of 100 mTorr. The shaft was lowered to puncture the bag of the pouch cell (not through the jelly roll). The low pressure in the chamber forces the gas out of the pouch cell inside the chamber, along with any high vapor pressure compounds potentially formed during battery use. The chamber was then back-filled with argon to equilibrate the pressure inside and outside the chamber. The gas from the chamber was then extracted from the chamber using a gastight syringe.

The extracted gas was then injected in the GC-MS. The GC-MS used was a Bruker 436-GC equipped with a split/split-less injector and a Q-PLOT (Bruker) 30 m column with an inner diameter of 0.25 mm and a coating thickness of 8 μm. Helium was used as carrier gas at a constant flow rate of 1.0 mL/min. The GC was coupled to a Bruker Scion single-quadrupole mass spectrometer equipped with an electron impact ionization module. The injector temperature was set to 250°C and the oven temperature was programmed to get the best component separation in the shortest amount of time. A high injector temperature was used to ensure the complete removal of non-gaseous compounds and prevent carry-over from one injection to the next. The end of the oven temperature cycle was set to 250°C for 5 min to ensure the elution of heavier highly retained compounds (mostly compounds

coming from septum bleed). The transfer line was set to 250°C, the ion source to 250°C and the electron energy to 70 eV. The MS used did not allow for the detection of hydrogen since it had a lower mass detection limit of 10 amu. The column used and the minimum oven temperature available on this instrumental setup did not allow the separation of O_2, N_2, and CO, therefore the mass spectrometer was set to a single ion monitoring mode (SIM) for the measurement of these three gases during the first 3 min of the oven program and to a full scan mode for the rest of the oven program. Since CO and N_2 have similar principal ionic mass (m/z of 28), CO was monitored using the fragment with a m/z of 12 (0.5% of the intensity of the principal ion).

2.3.3 Results and Discussion

Figure 2.4 shows the volume change (Δv) of pouch cells charged to 4.7 V and then left on open circuit. The change in volume at a given time is taken between the start of the charging process and the given time, or equivalently, after the 24 h 1.5 V wetting procedure and the given time. All cells, in all three sets of panels, show two distinctive gas productions steps: a low voltage step, which occurs around 3.7 V, and a high voltage step, which occurs around 4.3 V. The readers are reminded that these cells have sufficient graphite in the negative electrode so that Li plating does not occur, even at 4.7 V, so the high voltage gas step is not caused by lithium plating.

Figure 2.4: In situ gas evolution of NMC/graphite cells with control, 2% VC and 2% PES electrolytes at 25℃, 40℃ and 70℃. Voltage profiles are shown in the top row and volume change in the bottom row. This data was collected for the first charge, or formation, of the cells.

Between these two steps is a gas consumption feature, more noticeable for VC and PES than for control cells. There is also gas consumption after the second gas step. Higher temperature, in all cases, causes a larger volume change, for both steps. The results reveal that cells with 2 wt % PES electrolyte produce less gas than the cells with control electrolyte or the cells with 2% VC when charged to 4.7 V. Certain cells are shown with duplicate experiments to illustrate the reproducibility of the data.

Figure 2.5, in the first column of panels, shows the chromatogram of the gas extracted from pouch cells after being charged to 3.7 V or 4.7 V. The gas peak identifications were made based on the mass spectra associated with each step. In the second column of Figure 2.5, the area of the GC-MS peaks for compounds gaseous at room temperature was integrated and normalized in order to obtain a quantitative estimate of the relative composition of the gas mixture for gases other than H_2 in each cell. The first gas step was studied for control, VC and PES using GC-MS data of cells charged at 3.7 V (top row panels in Figure 2.5). For the second step, cells were charged to 4.7 V before being analyzed by the GC-MS (bottom row panels). For the first gas step (3.7 V), ethene is the most abundant gas, as shown by the top right panel. This gas was likely formed by reactions involving the solvent and the graphite negative electrode, such as in Figures 1.3 and 1.4. Previous scholarship has argued that EC can produce ethene through reduction on the anode.[42] Also, EC does not produce any noticeable amounts of ethane, but the linear carbonate DEC can.[42] Thus, it is possible that the ethane results from reactions involving the linear carbonate EMC and the negative electrode.

VC hinders ethene production since the fractional amount of ethene is less for VC-containing cells and the volume change is dramatically reduced compared to control electrolyte for the first step. Namely, with 2% VC, at 3.7 V, there is a volume increase of 0.30 mL, while for control, it is 1.17 mL. This is consistent with suggestions that VC is preferentially reduced over EC on the negative electrode to form a SEI[18,43] which can prevent gas otherwise formed by reactions between EC and the negative electrode. PES also reduces the amount of ethene produced. This may indicate that PES participates in the

26

formation of the SEI at the negative electrode. Here, the total volume change at 3.7 V is about 0.18 mL. Also, the compound propene is identified for the PES-containing cells, but due to its low signal is perhaps simply produced during a side reaction involving the formation of the SEI. CO_2 in this first step could have been formed from water impurities as suggested by the following reaction:[36]

(2.2) $2ROCO_2Li + H_2O \rightarrow 2ROH + Li_2CO_3 + CO_2$
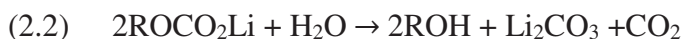
Due to a low signal to noise ratio, certain compounds could be present in very small quantities (less than 0.01% of the sum of peak areas) but are not shown in the second column of Figure 2.5, e.g. propene in cells with VC.

For the second step (4.7 V, bottom panels in Figure 2.5), CO_2 becomes the most abundant gas in the cell. The bottom right panel shows that CO_2 at 4.7 V is comparable in relative amounts for all cells (control, VC and PES). However, after the second gas step at 4.7 V, the total volume change for control, VC and PES are respectively about 1.49 mL, 0.90 mL and 0.30 mL. It is possible that the CO_2 is largely caused by the oxidation or decomposition of EC[42] or of certain species that make up the SEI present on the positive electrode.
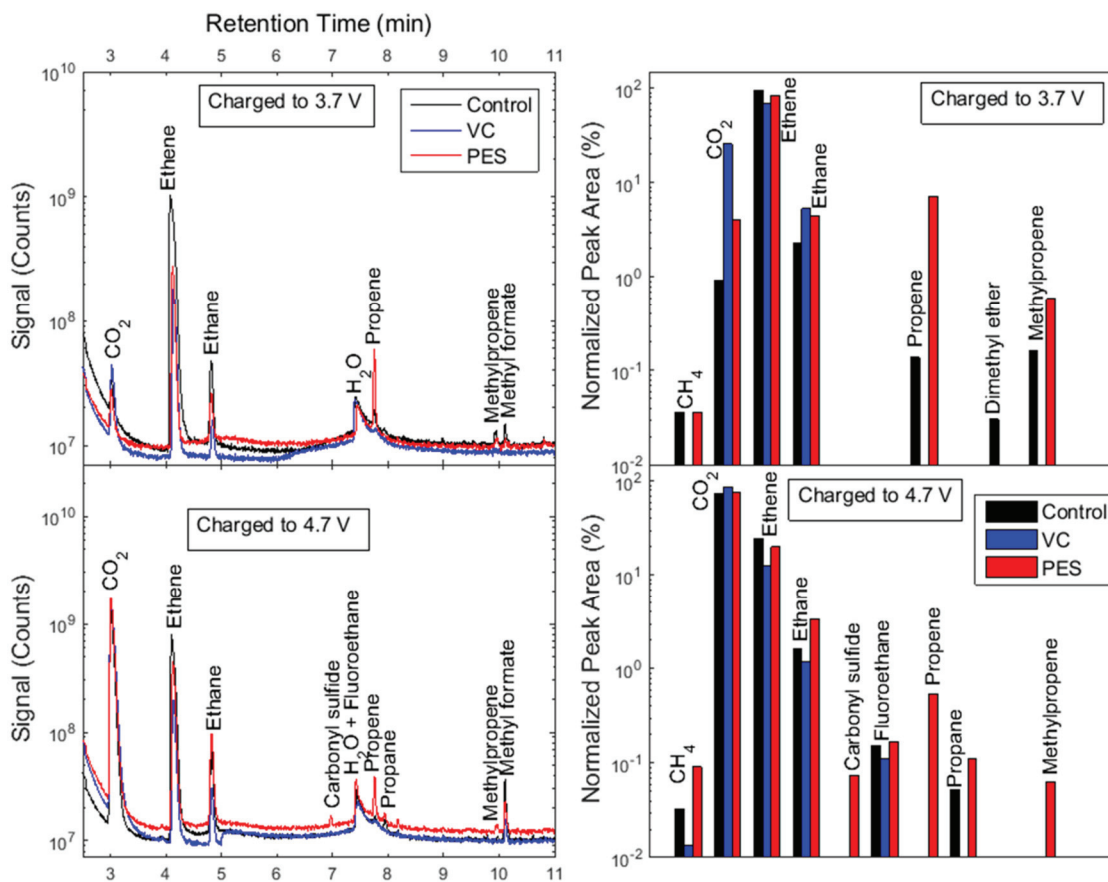
Figure 2.5: GC-MS data for gases collected from NMC/graphite cells with control, 2% VC and 2% PES electrolytes. The first column shows the signal counts as a function of retention time for cells opened at 3.7 and 4.7 V. The second column shows the normalized peak area for compounds that are gaseous at room temperature.

The precise mechanism by which EC can produce CO_2 is still unknown, but there have been many suggestions. The idea that a single or even two EC molecules can be oxidized (i.e. EC loses an electron) has been proposed and treated in recent DFT computation papers.[40,41] However, the oxidation potentials calculated (well above 5.5 V) are much higher than the operating voltage of the cells studied here (4.7 V) for which CO_2

was observed. No quantum chemistry calculations have been undertaken to evaluate the proposition of high voltage degradation of PEC (poly ethylene carbonate), a mechanism which, as explained in Chapter 1, may perhaps be the main formation pathway of CO_2. Anyhow, Onuki et al.[42] used ^{13}C labelled solvents in order to determine that a majority of the CO_2 produced in Li-ion cells came somehow from EC, and a smaller fraction came from the linear carbonate DEC. Metzger et al. also showed that the carbon black[44] in the positive electrode can produce CO_2 at high voltage.[45]

The bottom panels in Figure 2.5 show that carbonyl sulfide is produced in the cells containing PES charged to 4.7 V. This may suggest oxidation of PES at the positive electrode, creating the fragment carbonyl sulfide, which is similar to CO_2 from the oxidation of EC. For both the 3.7 V and 4.7 V gas step panels, the water is likely to arise from air as blank injections always show this water peak. Also, it is worth noting that for the second step, the gases other than CO_2, ethene and ethane are in very small quantities as the right column of panels in Figure 2.5 uses a logarithmic scale. The gas dimethyl ether probably arises from reactions involving the solvent component EMC.

The first gas step in Figure 2.4 around 3.7 V is likely largely due to the negative electrode, not only because of identification of gases tied to the anode such as ethene,[36,42] but also, when the same experiment was carried out for a different positive electrode (NMC442 coated with $LaPO_4$), the first step remained the same while the second step changed in its shape, as can be seen by comparing Figures 2.4 and 2.6. The second step is likely due mainly to reactions involving the positive electrode and solvent.
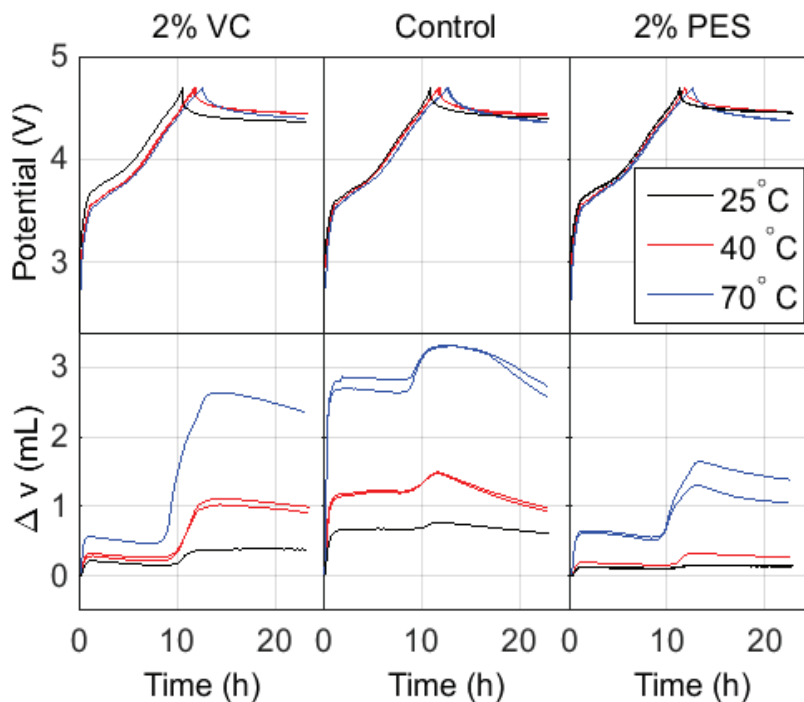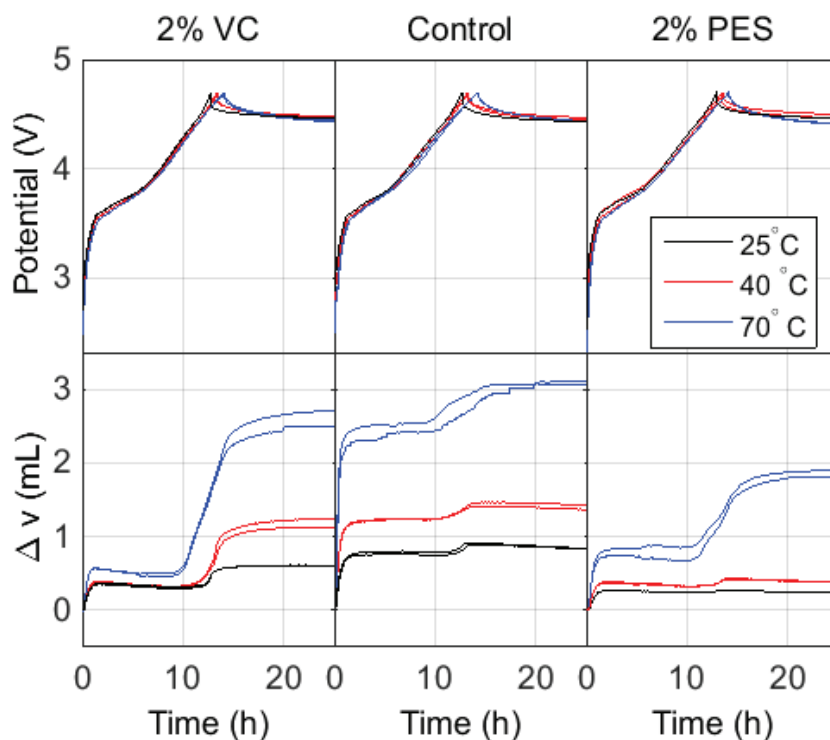
Figure 2.6: In situ gas evolution of LaPO₄-coated NMC/graphite cells with control, 2% VC and 2% PES electrolytes at 25°C, 40°C and 70°C. Voltage profiles are shown in the top row and volume change in the bottom row. This data was collected for the first charge, or formation, of the cells.

This is further supported by the identification of CO_2 as the main produced gas in this second step.[42]

Figure 2.7 shows the voltage versus capacity data for half cells, where the NMC442 cathode and graphite anode are studied against a pure Li electrode counterpart
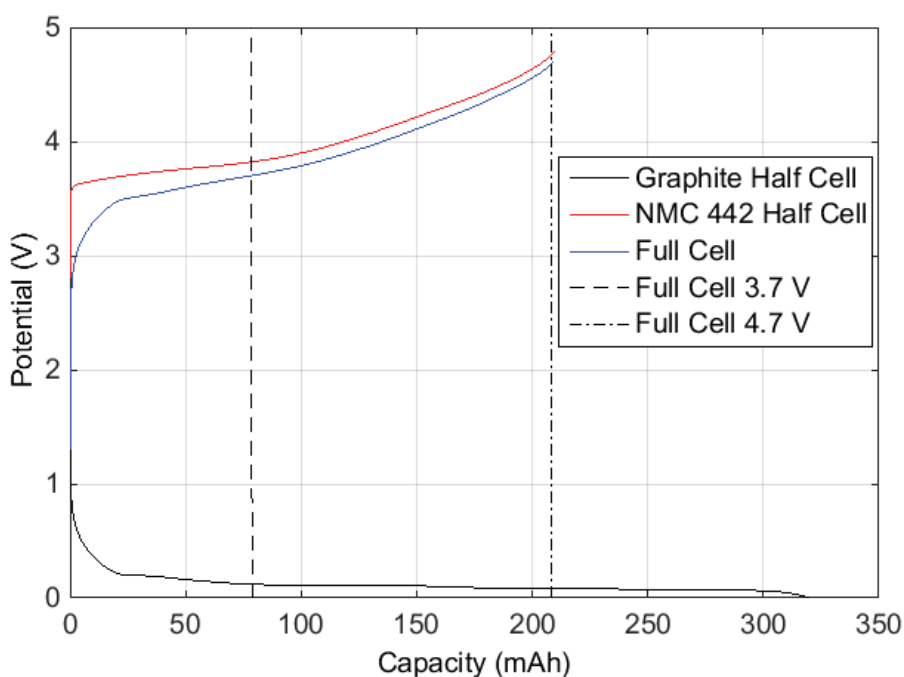
Figure 2.7: Half-cell voltage-capacity curves for NMC442 positive electrode and graphite negative electrodes used in these pouch cells. The full cell voltage capacity curve is also shown.

as well as the full Li-ion cell voltage capacity relation. This allows inspection of the voltage for a given electrode with regards to the full cell voltage. When the full cell is at 4.7 V, the graphite half-cell voltage curve is flat, which implies that the reactions due to the change in voltage are occurring on the cathode. In other words, Figure 2.7 further supports the claim that the second gas step is due to the cathode.

In order to determine whether the gas consumption feature for VC was a mechanical or an electrochemical process, fresh cells before formation with 2% VC were held at various voltages from 2.2 to 3.4 V. Figure 2.8a shows cells held at 2.2 V (black), 2.5 V
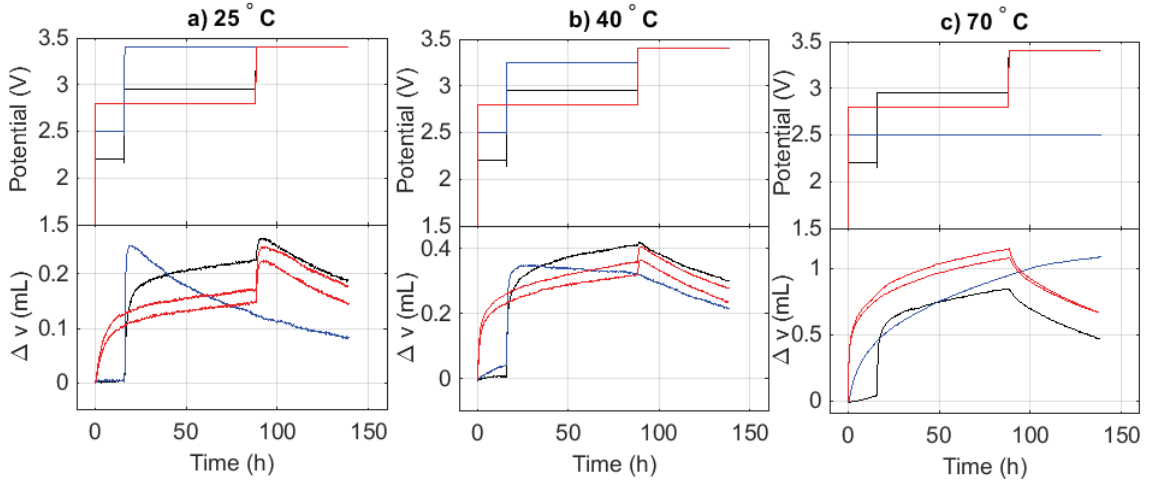
Figure 2.8: In situ gas evolution of NMC442/graphite cells with 2% VC electrolyte at a) 25℃, b) 40℃ and c) 70℃. Voltage profiles are shown in the top row and volume change in the bottom row. This data was collected for varying charging protocols, after an initial 24h holding procedure at 1.5 V. For each given temperature, a different colour indicates a different charging protocol. Cells held at 2.8 V and then charged to and held at 3.4 V are shown in red. Cells shown in black were charged to and held at 2.2 V, then 2.95 V and then 3.4 V. Cells shown in blue, were charged to and held at 2.5 V to 3.4 V in a), 2.5 V to 3.25 V in b) and 2.5 V in c).

(blue) and 2.8 V (red). The former two were then increased to 3.0 V (black) and 3.4 V (blue), and finally all cell voltages were increased to 3.4 V (red, black and blue). Assuming gas production doesn't decrease with cell voltage (from 2.5 V to 3.4 V), gas consumption is most evident at 3.4 V. This is true either for the cell that was the first to be held at 3.4 V (blue), or the other cells for which the voltage was held at 3.4 V about 100 h later (red and black). This may be an indication that at least some gas consumption is a function of

32

voltage. Similar results were found at 40°C and 70°C, shown in Figures 2.8b and 2.8c. It can be assumed that that at 25°C the gas produced at all voltages regimes shown in Figure 2.8a is mostly ethene (a fair estimate is 95%, as in the GC-MS results for cells charged to 3.7 V at 40°C, provided H_2 presence is minimal). Such an estimate implies that at least some ethene has to be consumed since more than half of the gas is consumed over a 100 h period.

It is still unknown whether the nature of the gas being consumed after the second gas step, as seen in the bottom row of Figure 2.4 after 12 h, is the same as the gas consumed after the first gas step. Furthermore, whether different electrolyte mixtures (control, PES) result in the same gas consumption mechanism as with the VC additive is also unknown and investigation should be subject of future work. However, the suggestion from Aurbach et al. of polymerized ethene on the negative electrode from EC containing mixtures[16] has been to some extent validated by XPS detection of polyolefins on graphitic SEI's.[11,46] Furthermore, Sloop et al. have also argued that CO_2 can be reduced at the anode to form Li_2CO_3, CO and hydrocarbons.[47]

2.4 Dissolution of Gaseous Species

Linear and cyclic carbonates can dissolve so much CO_2 that they are being considered as potential candidates for carbon capture and storage.[48] Thus, it is worth considering not only the amount of gas in the gaseous state but also the amount of gas dissolved in the electrolyte. This subsection will use reported values of Henry's Law

constants to get an estimate of the moles of gas in solution and in the gas phase for cells with 2% VC and control electrolytes at 25°C, 40°C and 70°C.

For a given gaseous compound in a Li-ion pouch cell, a certain number of moles of the gas will be dissolved in the electrolyte while the remaining will be in gas phase. Thus it can be written for a total number of moles of gas n_t:

(2.3) $n_t = n_g + n_s$

In equation 2.3, n_g is the number of moles of gas in gas phase and n_s the number of moles dissolved in the liquid solution. The ideal gas law can be written as:

(2.4) $Pv_g = n_gRT$

In equation 2.3, P is the pressure of the gas, v_g the volume, n_g the number of moles, R is the gas constant and T is the temperature. Henry's law can be stated as the following:

(2.5) $kP_x = n_s/v_s$

In equation (2.5), k is a temperature dependent parameter in units of $\frac{mol}{L\,atm}$ where 1 atm=101.325 kPa. n_s/v_s is the concentration of dissolved gas in units of $\frac{mol}{L}$, v_s is the volume of the electrolyte solution and P_x is the partial pressure of the gas. If a gas mixture is only comprised of one gas, the partial pressure is equal to the actual pressure of the gas: $P = P_x$. In this case, equations 2.4 and 2.5 can be substituted into 2.3:

(2.6) $n_t = Pv_g/RT + Pkv_s$

Thus, for a single gas in a Li-ion cell, the number of moles of gas can be calculated provided the pressure, the volume by which the cell has expanded, the temperature, Henry's constant for the electrolyte mixture and the volume of the electrolyte mixture are all known.

For both gas steps, as shown in the bottom-center panel of Figure 2.4, equation 2.6 can be used, albeit with certain assumptions and approximations. The validity of these will be discussed later on. It can be assumed that there is one gas (CO_2 after the 2nd gas step). Furthermore, the pressure can be taken as 1 atm. The volume of the electrolyte mixture v_s can be taken as 0.8 mL. v_g is measured by the MAGE device, and, for the gas CO_2, k can be found in work by Dougassa et al.[49] Unfortunately, reported Henry's constants are dimensionally different depending on the source.[49–51] A different formulation of Henry's law, with Henry's constant k' can be written:

(2.6) k'=P/y where k' is in units of MPa

Here, y is the mole fraction of gas in solution (e.g. the mole fraction of say dissolved CO_2 in the electrolyte solution). k can be related to k' using

(2.7) $k=n_{bulk}/k'$

where n_{bulk} is the number of moles/L for the bulk solution (i.e. the inverse molar volume of electrolyte) in which the gas is dissolved. For the control electrolyte (EC:EMC 3:7), n_{bulk} = 11 mol/L. Separately, EC and EMC are 15.0 and 9.7 mol/L, respectively.

Figure 2.9 shows k(T) for CO_2 using the tabulated values for k'(T) from Dougassa et al.[49] and equation 2.7. Notably, CO_2 is less soluble in water than it is in EC with and

35

without $LiPF_6$, EMC with and without $LiPF_6$, and mixtures of EC:EMC with $LiPF_6$. The average for EC:EMC 1:1 was computed from the Henry's constants of the individual co-solvents (with salt, i.e. 1 M $LiPF_6$) in order to assess the validity of taking a linear average. Since the agreement is good between EC:EMC 1:1 w/ salt calculated from an average of the experimental fits, an average was also taken for the control electrolyte (shown in black circles).

Using k for 25ºC, 40ºC and 70ºC, equations 2.3, 2.4 and 2.5 and v_g from the data shown in Figure 2.4, the number of CO_2 moles for cells with VC after the formation can be computed. The second gas step, where mostly CO_2 is produced, is more evident for VC than for PES or control cells. Moreover, the increase of this gas step with temperature is most significant for VC, as is shown in Figure 2.4.

The gas in VC cells is mostly CO_2 (> 85% moles of CO_2 as in Figure 2.5), and since most VC gets consumed during charge,[52] the k values for the control electrolyte are arguably reasonable to use. Figure 2.10 a shows n_g, n_s and n_t for the VC second gas step at different temperatures. It is clear that for a given number of moles, an increase in temperature results in an increased measured volume v_g: the gas in gaseous phase expands while the electrolyte can dissolve less gas before saturation. In Figure 2.10 a, the total moles of CO_2 n_t increases from 0.10 to 0.11 to 0.13 mmol for 25ºC, 40ºC and 70ºC. This increase is not nearly as pronounced as the increase in measured volume change v_g, which goes from 0.4 to 1.1 to 2.6 mL for 25ºC, 40ºC and 70ºC, respectively.

36
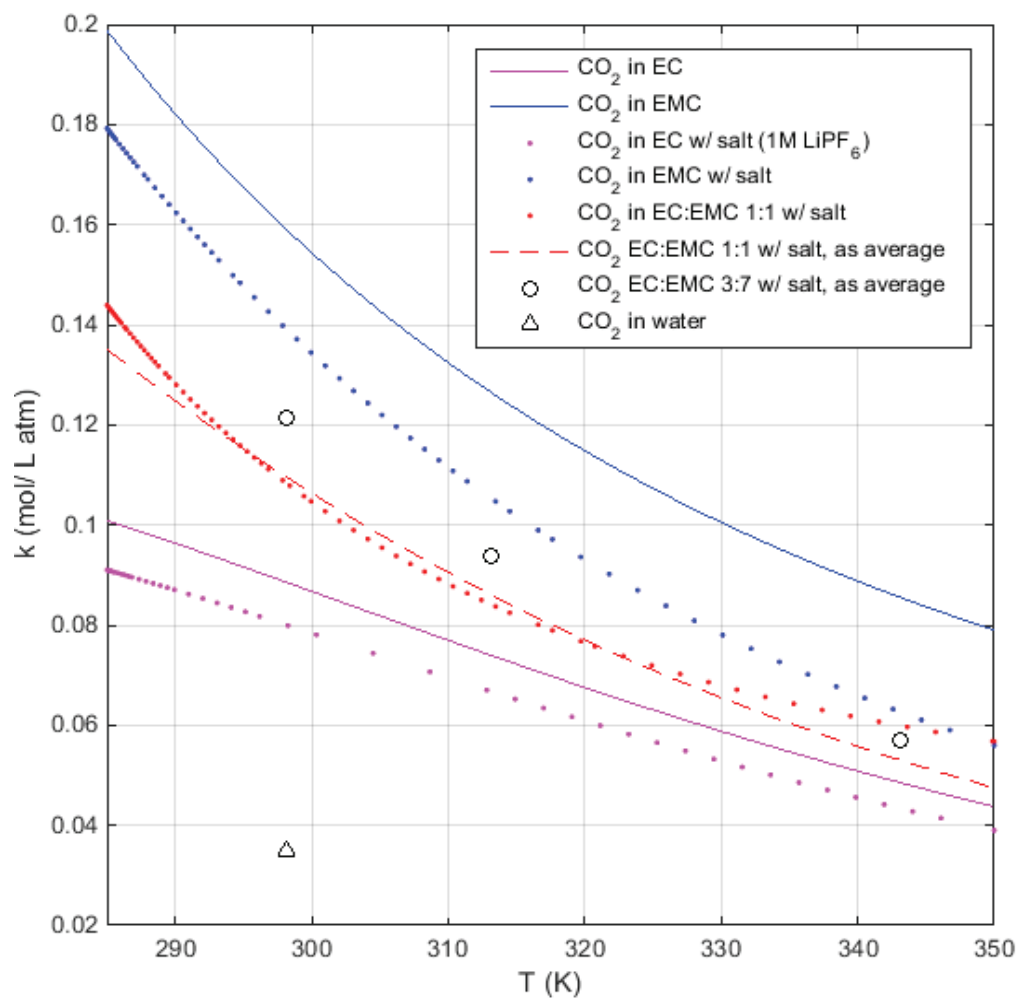
Figure 2.9: Henry's constants for dissolution of CO_2 into water (triangle, datum taken directly from NIST)[51] and cyclic carbonates. Extrapolated $k=k(T)$ functions either directly reported from Dougassa et al.[49] as k', or taken as an average from individual solvent components in a given mixture. k is in units of mol/(L atm) and k' is in units of MPa.
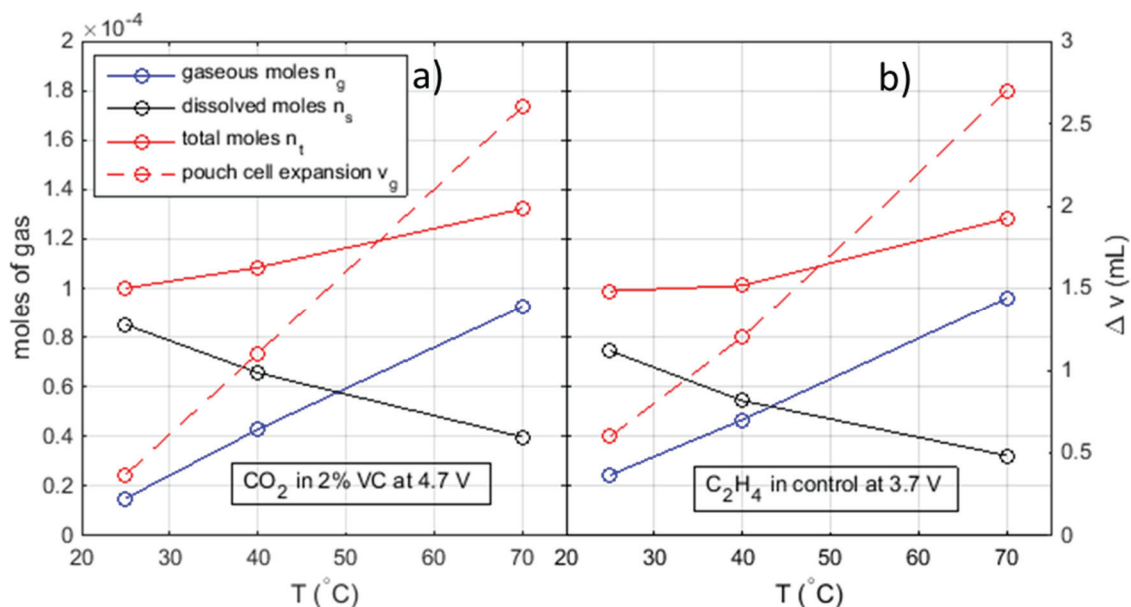
Figure 2.10: a) Estimate of number of moles of CO_2 in cells with 2% VC after the first charge while taking into account dissolution of gas. b) Estimate of number of moles of C_2H_4 in control cells after the first charge while taking into account dissolution of gas.

There are a few caveats: the pressure was assumed to be 1 atm, although perhaps the exact pressure in a pouch cell increases with the amount of moles of gas, even before significant swelling and stretching of the flexible casing (e.g. v_g between 0.1 and 3 mL). Furthermore, perhaps the nature of the gases changes dramatically from 25 °C to 40 °C and/or from 40 to 70 °C. Also, the presence of H_2 may be significant and unaccounted in this treatment. Possible further work should intend to clarify all of the above mentioned points.

The same treatment can be undertaken for the first gas step, where ethene is the dominant gas. In cells with control, at 40°C, the gas is mostly ethene (> 95%, as in Figure 2.5), and ethene has both the largest first gas step and increase in first gas step with temperature compared to VC and PES, as shown in Figure 2.4. From, Dougassa's 2014

38

Thesis,[53] values for dissolution of C_2H_4 in EC and EMC can be found, but only without salt (data from Dougassa's Figure III 14). As shown in Figure 2.9, the salt does not change k values by more than ~15% for CO_2 and so k for C_2H_4 dissolution in EC:EMC 3:7 can arguably be taken as an approximation for C_2H_4 dissolution in EC:EMC 3:7 with salt. For 25ºC, 40ºC and 70ºC the k values for C_2H_4 dissolution, taken as the average from k of the individual co-solvents, are 0.11, 0.078 and 0.046 mol/(L atm) respectively. Figure 2.10b shows n_g, n_s and n_t for the control first gas step at different temperatures. Once again, n_t (solid red), increases with temperature but in a much less pronounced manner than the change in volume v_g does (dashed red). For example, from 25ºC to 40ºC, or 25ºC to 70ºC, n_t goes up by 1% and 30% respectively, while for v_g the increase is by 100% and 350%, respectively. Thus, v_g should not be used alone to evaluate to what extent different temperatures increase gas production in terms of moles.

2.5 Pouch Cell Leakage

The Li-ion cells studied in this chapter had a pouch made up of aluminum, with an inner polypropylene layer and outer polyamide layer, similar to pouch cells from other laboratories.[54] During sealing, the two inner polypropylene layers were melted together. It is assumed here that gas permeation either out of or into the cell happens occurs through this polypropylene barrier, and, not through any aluminum. This subsection is a preliminary investigation as to whether gas permeation is significant enough to directly affect MAGE measurements.

For polypropylene, while considering H_2, water, CO_2, O_2 and N_2, H_2 has the largest permeability coefficient by an order of magnitude when T$\sim$25°C.[55] Thus permeation of H_2 can serve as an upper bound on any of these gases leaking into or out of a cell. Units of permeability can be expressed as cm^3 mm/ (m^2 day atm), or, volume of gas × thickness of membrane / (area of membrane × time × pressure).

For the pouch cells in question, the thickness of the membrane, or path length of the permeating gas, is 5 mm. Given a perimeter of 100 mm, the area of the polypropylene membrane is 0.1 mm × 100 mm = 10 mm^2. 0.1 mm is a common size for the polypropylene layers in Li-ion pouch cells.[54] 1 atm pressure can be used for calculation of an upper bound for gas leaking into or out of the pouch-cell. For H_2, the permeability is 2700 cm^3 mm/ (m^2 day atm) at STP (Standard temperature and pressure).[55] Thus, the amount of gas permeating in one day can be calculated:

$$2700\frac{cm^3\ mm}{m^2\ day\ atm} \times \frac{1\times10^{-5}m^2 \times 1\ atm}{5\ mm} = 0.005\ mL/day$$

Since, during the first charge, the pouch cells show volume changes of $\sim$ 1 mL, the amount of gas permeating into or out of the cell on the time scale of days is insignificant, provided leakage would occur through the polyprolyene.

The water permeating into a cell during a year can also be estimated. The permeability coefficient for water vapour is 335 cm^3 mm/ (m^2 day atm).[55] At RT, the partial pressure of water is typically about 3000 Pa $\approx$ 0.03 atm at 100% RH.[56] This gives 0.007 mL/year, which is but a trace amount of water and would not be detected with the MAGE

apparatus. Sven et al. found, through their experimental setup, an upper bound of water leaking into pouch of comparable dimension of 0.02 mL/year.[54]

Further work should investigate whether electrolyte solvents can somehow react over large time scales with the polypropylene layer and subsequently, with the Al layer, which has been raised as a concern.[57] However, reference 57 shows that commercial pouch cell material from Sumitomo Electric, which is similar to the material in the LiFUN pouch cells, is incredibly good, leading to less than 1% electrolyte weight loss from pouch cells continuously thermally cycled between -40 and +60°C after 15 years (extrapolated).

Chapter 3: The Role of Prop-1-ene-1,3-Sultone as an Additive

(The work and writing in this chapter, as well as in Appendix A, was an equal contribution collaboration between Julian Self and David S. Hall under the supervision of J. R. Dahn. Lénaïc Madec completed the experimental XPS work. A large portion of this chapter has been submitted to the Journal of Power Sources for publication)

3.1 Introduction

One way to improve lithium-ion battery (LIB) charge-discharge cycling performance and lifetime is the use of electrolyte additives. Certain compounds added to the electrolyte solution on the order of a few weight percent can significantly extend cycling and calendar lifetimes, reduce detrimental gas formation in cells, and/or improve LIB safety.[2,5,12,33]

The electrolyte additive studied here is prop-1-ene-1,3-sultone (PES), which has received considerable attention in recent years for its use as an individual additive and as a part of binary and ternary blends.[25,58–64] PES has been shown to reduce gas production at both electrodes during the first charge, commonly called the formation, and during charge-discharge cycling.[25,33,65] Moreover, PES prevents destructive exfoliation of the graphite anode.[5,25] This may indicate that PES is a film-forming additive that produces a stable barrier layer on the graphite surface, known as a solid electrolyte interphase (SEI). Charge-discharge cycling experiments and surface analysis studies have provided further clues for understanding the fate of PES in cells.[60,61] However, the reactions of PES at the electrodes and the nature of the resulting SEI remain uncertain. More generally, it is a standing

42

problem that the exact role of most electrolyte additives are unknown. Clearly developed methods to follow the decomposition of additives in a battery would be of significant benefit to the field.

In this work, several possible electrochemical and chemical reaction pathways of PES in a LIB are mapped. Computational chemistry is applied to make predictions that can be tested and compared with experimental results, many of which are already available in the published literature. The overall goal of this work is not only to understand the role and ultimate fate of PES in LIBs, but also to establish methods that may be applied to related compounds for the intelligent design of new and improved electrolyte additives.

3.2 Calculations

Quantum chemistry calculations can allow determination of thermodynamics and kinetics of given chemical reactions by using numerical (approximate) solutions to Schrodinger's equation. If the total of the free energies of the products are less than for the reactants, the reaction is thermodynamically favourable (exergonic). Also, the size of a given energy barrier, e.g. from a transition state (TS), allows inference of kinetic favourability (i.e. the speed of a reaction).[66]

The precise details of the approximation schemes to Schrodinger's equation are out of the scope of this thesis. Briefly, the total potential, which includes coulombic interactions, also includes the so-called exchange potential and correlation potential to account for the density of molecular electronic orbitals.[67] The total potential is approximated by what is called the functional. One way to implement the functional is by

using Gaussian-type orbitals (GTO) for the so-called basis set. The basis set uses linear combinations of atomic orbitals (LCAO) to model the electronic density contribution from individual atoms to the molecular orbitals' energies. In order to account for solvation, one approach is to use to use the integral equation formalism variant of the polarizable continuum model (IEFPCM),[68] which models the solution as a dielectric medium and calculates the interaction energy with the solute molecule, placed in a given cavity where the dielectric constant $\varepsilon=1$. By modifying the atomic positions of a given molecular complex, the total electronic energy can be mimized for a stable (or metastable) "relaxed" structure. Such a minimum is a local minimum in the potential energy surface, for which a local maximum along one degree of freedom (i.e. reaction coordinate) may constitute a transition state.

For the calculations in this thesis, the hybrid functional B3LYP[67] was used with the 6-311++g(d,p) Pople basis set[69] in the Gaussian quantum chemistry software package (G09.d01).[70] The IEFPCM-UFF solvation model was used[68] with the dielectric constant set to 20 as a good representation of the 3:7 binary mixture of EC and EMC (ethylene carbonate and ethyl methyl carbonate, ratio by weight, without salt) near room temperature.[71] Except where noted, energy diagrams show the Gibbs free energy of reaction calculated in solution and at 25°C. Stable and metastable geometries were all tested by vibrational mode analysis and have only real (positive) vibrational frequencies. Transition states all have only one imaginary (negative) vibrational frequency. Standard potentials are all reported relative to the Li/Li^+ electrode in the same solution (i.e., $\varepsilon = 20$). Further details can be found in Appendix 1.

3.3 Results and Discussion

3.3.1 Gas-phase Decomposition Products

The strategy adopted for this research was to first examine published decomposition products that have been either proposed as theory or experimentally observed (see Chapter 2). Table 3.1 summarizes these published decomposition species.[59,60] Next, retrosynthetic analyses and density functional theory (DFT) calculations were performed to map out possible reaction pathways that would result in the production of these byproducts. It was borne in mind that those pathways that result in the observed products (e.g. propene) should be more favourable, either thermodynamically or kinetically, than those pathways that result in the products that are not experimentally observed (e.g., propyne). That is, the free energies of reaction should be more exergonic and/or the transition state barriers should be smaller. Notably, carbonyl sulfide (OCS) must form directly from the decomposition of PES. As described in Chapter 2, this species was observed by GC-MS while PES was the only source of sulfur atoms in the studied cells. Therefore this investigation begins with the study of OCS.

Table 3.1 : Proposed and experimentally observed PES decomposition products. The presence of each species in the GC-MS reported in Chapter 2 is indicated for cells prepared with and without PES.

Compound Name	Formula	Structure	GC-MS PES	GC-MS Control	Proposed Pathway
Carbonyl sulfide	OCS	O=C=S	●	×	Path B
Ethene	C_2H_4		●	●	Path B
Propene	C_3H_6		●	●[a]	Path E
Methylpropene	C_4H_9		●	●	Path E
Propane	C_3H_8		●	●	Path E
Propyne	C_3H_4		×	×	[7,8], Path D
Cyclopropene	C_3H_4		×	×	[8]
Oxygen	O_2	O-O	---[b]	---[b]	Path A

[a]This species was significantly more abundant in cells that contained PES than in control cells.

[b]Not detectable by GC-MS; the presence of O_2 is therefore unknown.

3.3.2 Oxidation and Carbonyl Sulfide: Paths A and B

The OCS species was only observed in Li-ion cells that were charged to high cell voltage (E = 4.7 V), whereas it was not present in cells that were only charged up to 3.7 V

(see Chapter 2).   It has previously been shown that the potential at the negative electrode does not change significantly between these cell voltages. Therefore, the potential at the positive electrode increases by nearly 1.0 V.[33] This is strong evidence that OCS forms from the decomposition of PES at the positive electrode surface at high cell voltage. It was therefore considered that OCS may be produced by the electrochemical oxidation of PES at the positive electrode surface. Thus, the oxidation of PES was modeled. The structure of neutral PES is shown in Figure 3.1. The removal of an electron from PES elicits a shortening of the C–S bond, while the other bond lengths change by a few percent or less (Table 3.2).
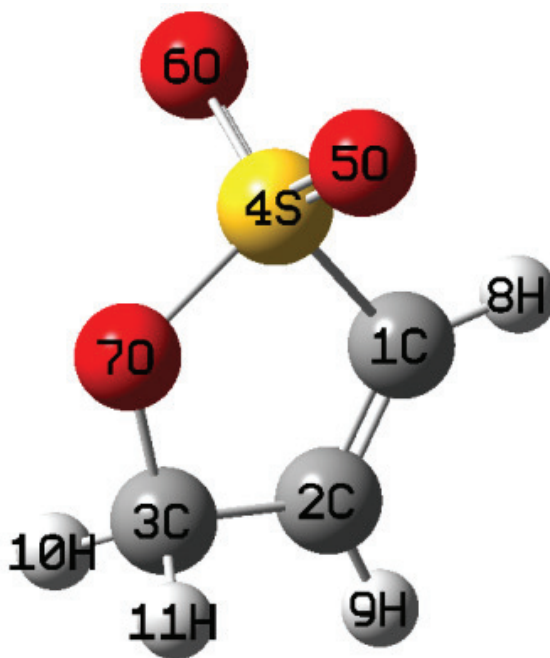
Figure 3.1: Ball and stick representation of the PES molecule.

Table 3.2 : Bond lengths for neutral PES and singly oxidized [PES]⁺ molecules.

	PES	[PES]⁺	Δd (PES → [PES]⁺)	
	Å	Å	Å	%
1C–2C	1.324	1.368	0.044	3.3
1C–4S	1.775	1.462	-0.313	-17.6
1C–8H	1.079	1.082	0.003	0.3
2C–3C	1.498	1.462	-0.036	-2.4
2C–9H	1.082	1.083	0.001	0.1
3C–10H	1.092	1.106	0.014	1.3
3C–11H	1.092	1.106	0.014	1.3
3C–7O	1.448	1.42	-0.028	-1.9
4S–5O	1.460	1.453	-0.007	-0.5
4S–6O	1.460	1.454	-0.006	-0.4
4S–7O	1.651	1.647	-0.004	-0.2

The full chemical route from the singly oxidized [PES]⁺ cation (S1a) to OCS begins with the loss of the two out-of-ring oxygen atoms (Pathway A, Figure 3.2a). Although this was modeled as the loss of molecular O_2 from the structure, it is quite likely that this process is actually mediated by the positive electrode surface (*i.e.*, $Li_xM_yO_2$, M = Ni, Mn, Co) and may be a multistep process. For example, the bond dissociation reactions of gas-phase H_2 and O_2 have large activation energies (~4.1 – 4.4 eV/400 – 420 kJ mol⁻¹ and 4.6 – 4.8 eV/440 – 460 kJ mol⁻¹, respectively) hence both species are stable at room temperature.

48

However, the dissociation to form adsorbed surface species occurs very rapidly with little barrier to reaction on a variety of transition metal and metal oxide surfaces.[72] This is attributed to the mixing of the diatomic σ-bonding orbitals with empty d-orbitals at the catalytic surface sites. Likewise, the large barrier for the spontaneous loss of the two oxygen atoms from S1a, $\Delta G^{\ddagger} \approx 3.6$ eV = 350 kJ mol^{-1} (Figure 3.2c, TS1a), is likely a poor representation of the reaction that takes place at the positive electrode surface. Clearly, further study would be required to fully understand the details of this proposed process. However, representation of a mixed transition metal oxide surface-mediated process is beyond the scope of the present work. Rather, that pathway A is indeed spontaneous is sufficient to conclude that this process may occur in a cell.

Next, a series of intramolecular steps results in a four-membered ring (MS3b) that dissociates to produce OCS and cationic ethene (Pathway B, Figure 3.2b). Cationic ethene may gain an electron either by reaction with other species in solution, or by reacting with an electrode. Therefore, Pathway B also predicts the production of ethene gas, which is another observed decomposition species in PES-containing LIBs (Table 3.1). Although the calculated activation energies along pathway B are quite high, intramolecular reactions such as ring opening and ring closing can occur much more rapidly than intermolecular processes that have the same activation energy.[73] Moreover, it is possible that these reactions are catalyzed by the positive electrode surface and/or ion-pairing with PF$_6^-$ anions in solution.[40] This would lower the transition-state energies but would not change the overall free energy change from S1 to MS4b. Therefore, the electrochemical oxidation of

PES at the positive electrode surface, followed by reaction pathways A and B, is a possible route that may explain the formation of OCS and ethene gases in PES-containing LIBs.
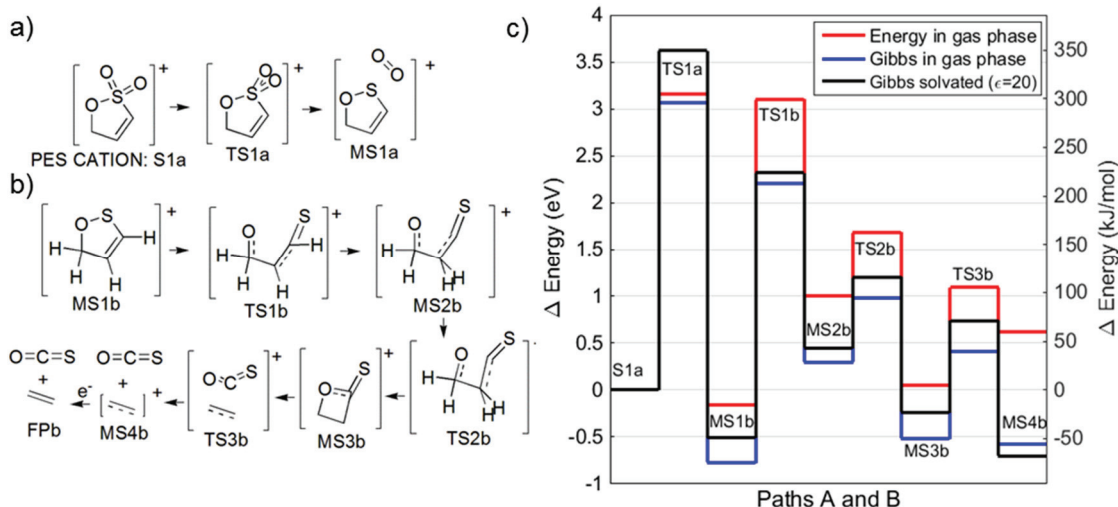
Figure 3.2: a) Reaction pathway A, b) reaction pathway B, and c) Free energy of reaction along pathways A and B.

Figure 3.2c also illustrates the importance of free energy and solvation in DFT calculations. When the electronic energy or free energy in the gas phase is examined, the final product (MS4b) is not the global minimum. However, when the reaction pathway was simulated again, this time using a solvation model, the experimentally observed final products (OCS and ethene) occupy the global free energy minimum, as expected. Many published works have previously approximated their systems as in vacuo[40,74] or failed to stress the importance of considering the free energy over the electronic energy.[40] Some work has been done that considered pure solvents.[15,39,41] However, most commercial and experimental cells contain binary or ternary solvent blends.[4,75] Accurate experimental

values for the dielectric constant, ε, to allow more accurate solvation energy calculations in the mixed EC/EMC solvent blends have recently been reported,[71] and the results in Figure 3.2c illustrate their importance for DFT simulations in LIB research.

3.3.3 Oxidation Potentials and the Reactive Electrode Model

The calculated oxidation potential of PES is $E^0 = 6.7$ V vs. Li/Li$^+$. This potential is quite high, given, as described in Chapter 2, OCS was observed in cells at just 4.7 V and so the accuracy of the calculation was examined.[76] First, the oxidation potential was calculated again using a higher level of theory and an expanded basis set. The M06-2X double hybrid functional was chosen, because it gives accurate ionization energies in vacuo[77] and was suggested by Borodin et al. for more accurate oxidation potentials.[76] The 6-311++g(2df,p) basis set was adopted, because the additional polarization functions may better represent any hypervalency effects on the S atom. Moreover, the oxidation potential was calculated both with and without ion-pairing with [PES]$^+$ and a [PF$_6$]$^-$ anion. However, the calculated standard potential for PES oxidation did not change from the originally calculated value by more than ±0.1 V.

Thus far, the species under study was presumed to singly oxidize and then decompose in solution. Such calculations involving oxidation processes remain a source of difficulty in LIB research. For example, the calculated potential of EC oxidation is ~6.5 V.[76] However, EC oxidation has been observed in Li-ion cells at much lower voltages (*e.g.*, below 4.7 V).[45,78] By contrast, the calculated potentials of oxidation for a group of potential shuttle molecules were calculated within ±0.15 V (mean-squared deviation), at a lower

level of theory than was used in this work.[79] It is unclear why certain oxidation potential calculations are very accurate whereas others, which use the same methodology, are not at all accurate. It is here proposed that the problem with these calculations may not lie with the DFT functionals or the basis sets. Rather, there may be a more fundamental problem with how the problem of oxidation in LIBs is being approached. It was therefore considered that the reaction itself may be the problem. Although a simple, one-electron oxidation in solution may work well for the organic shuttles studied by Wang et al.,[79] most of which were aromatic molecules, this may not be a reasonable approximation for PES oxidation (Table 3.3 – reaction 1). The calculated potential (vs Li/Li$^+$) for the full process, i.e. S1a to MS4b, is ~6.0 V (Table 3.3 – reaction 2). Although this is indeed less than the simple oxidation model, the result is still greater than 1.5 V above the voltage at which OCS, proposed to originate from PES oxidation, is detected.

Table 3.3 : Three models of PES oxidation and the calculated standard potential (vs. Li/Li$^+$)/free energy change of each.

(1) Simple oxidation:	$PES \rightleftharpoons PES^+$	E^0 = 6.7 V
(2) Full process:	$PES \rightleftharpoons O_2 + OCS + C_2H_4^+$	E^0 = 6.0 V
(3) Reactive electrode:	$PES + 2\,NiO_2 \rightleftharpoons 2\,NiO + 2CO_2 + 2H_2O + OCS$	ΔG = -6.11 eV

Finally, an alternative approach to the problem was considered. The possibility that the positive electrode material itself may participate in reactions is certainly not new. However,

the role that the positive electrode plays has focused on the cathode as a catalytic or an electrocatalytic surface. It is instead proposed that the positive electrode may rather adopt the role of a reagent. This concept is here termed the 'reactive electrode model.' At high cell potentials, the lithium near the electrode surface is depleted (Li_xMO_2, $x \to 0$, M = Ni, Mn, Co). At sufficiently low Li content, i.e., at sufficiently high cell potential, there is experimental evidence that the lithium metal oxide becomes unstable and loses oxygen to form a rock salt surface layer.[80–82] It is possible that the loss of oxygen may occur via the pseudo-combustion of PES, and/or other solvents, as shown in Table 3.3 – reaction 3. In this work, the mixed metal oxide was represented as a nickel oxide to simplify the estimation of the free energy of reaction. The free energy of this pseudo-combustion process is very exergonic (details in Appendix 1). A detailed analysis of this proposed pathway and the effects of such factors as the Ni, Mn and Co content of the electrode is beyond the scope of the present work. Future work may further examine this concept and how it applies to the solvent molecules and other additives.

3.3.4 PES Reduction-decomposition Pathways

The formation of the remaining gas-phase products in Table 3.1 via the reaction of PES with Li^+ and e^- at the graphite negative electrode was then considered. The addition of an electron to PES results in the accumulation of negative charge at the two out-of-ring oxygen atoms. This anion strongly associates with a Li^+ cation from the electrolyte solution or from the negative electrode to form the overall neutral species shown in Figure 3.3a (MS2c). The calculated standard potential is $E^0_{red,1} = 0.9$ V vs. Li/Li^+. This result was compared to the differential capacity peak at ~2.4 V that Xia *et al.* suggested corresponds
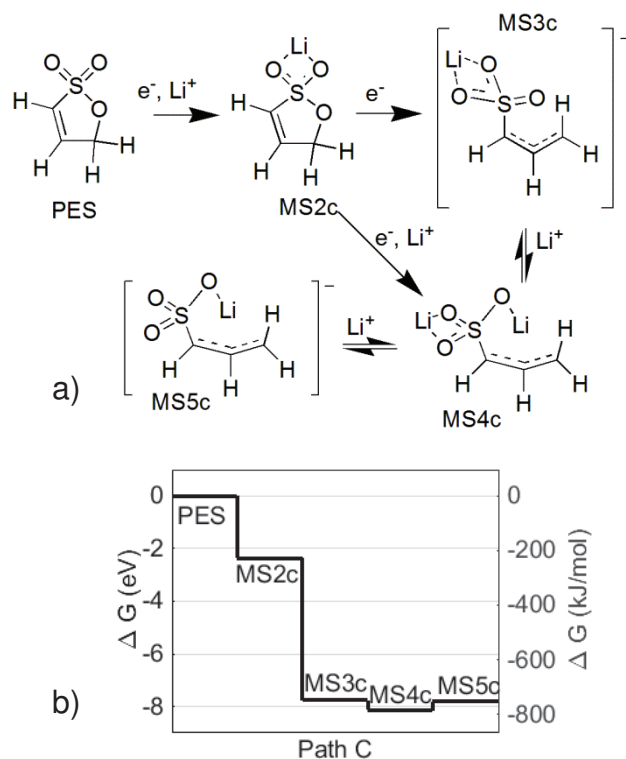
Figure 3.3: a) Reaction pathway C, involving two consecutive one-electron reduction steps of PES. The dissociation of the end product, Li$_2$PES, is shown. b) Free energy of the reaction steps in pathway C.

to PES reduction (Figure 3.4).[62] At this cell voltage, the positive electrode potential is ~3.5 V vs. Li/Li$^+$ (see Chapter 2). Therefore, the experimentally observed reduction peak is centred at ~1.1 V vs. Li/Li$^+$, which is an excellent match to the value calculated in this work. A second reduction step was modeled, which produces the organolithium compound shown in Figure 3.3a (MS4c). The fully associated Li$_2$PES compound is slightly more stable than either singly dissociated species (Figure 3.3b, MS3c, MS4c, MS5c). The standard potential for this second reduction process is E$^0_{red,2}$ = 4.3 V vs. Li/Li$^+$ (MS2c →

MS4c). That the standard potential is so positive indicates that the second reduction is very favourable and is expected to occur very rapidly.

It is essential to consider the proposed and observed gas-phase decomposition products to guide the computational modeling. Propyne has been repeatedly suggested as a likely decomposition product[59,60] and yet it has not been experimentally observed (see Chapter 2). Pathway D (Figure 3.5) was therefore considered, which results in the formation of propyne, as an energetic upper bound. That is, for a reaction to occur, the kinetics must be faster than pathway D.
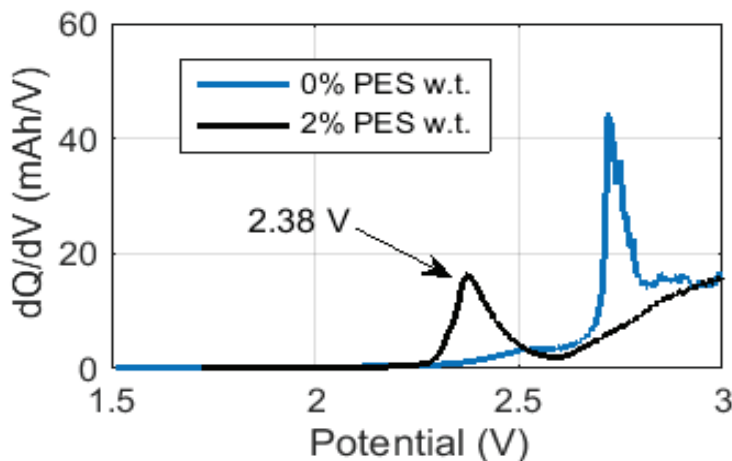
Figure 3.4: Differential capacity as a function of cell voltage for the first charge of Li(Ni$_{1/3}$Mn$_{1/3}$Co$_{1/3}$)O$_2$/graphite pouch cells (NMC 111) charged at constant current (C/20). Data courtesy of Xia et al.[62]
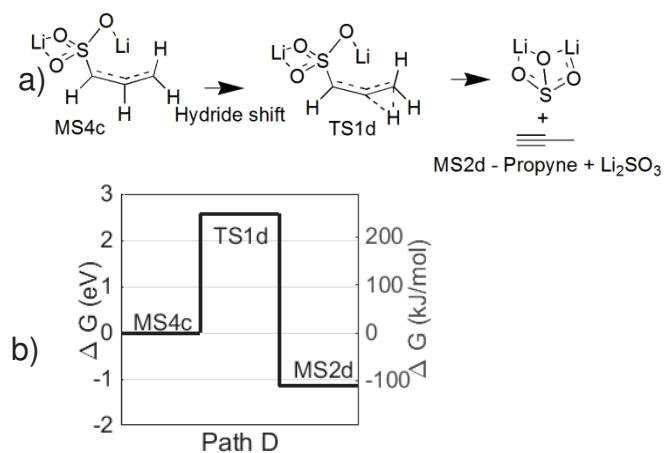
Figure 3.5: a) Reaction pathway D, b) Free energy of the species shown in (a).

The addition of just 2 wt % PES to a cell leads to an increased amount of propene generation (see Chapter 2). Looking at the structure of Li$_2$PES, it is apparent that the addition of two hydrogen atoms may yield this product. Although the source of hydrogen remains uncertain, there is evidence of radical species, including methyl and hydrogen radicals in LIBs during operation.[83] For simplicity, the reaction of Li$_2$PES with isolated H radicals to obtain the observed product propene was considered (Figure 3.6). Because both steps involve the addition of radical species, the activation energies are small and the reactions are very exergonic. Moreover, further reactions of propene with hydrogen and methyl radicals could produce propane and methylpropene, two other experimentally observed species in PES-containing cells (Table 3.1).

56
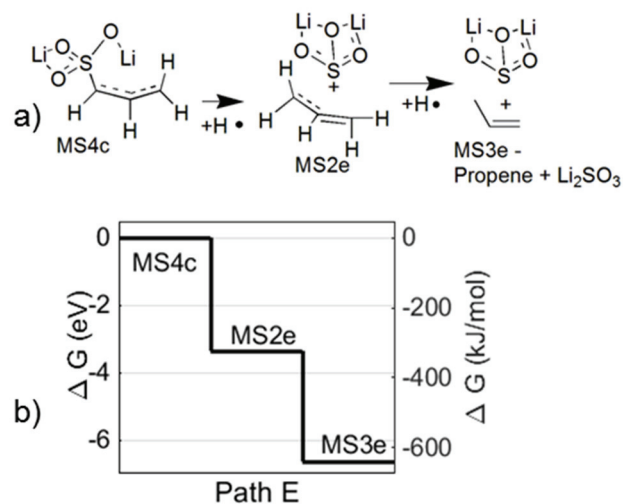
Figure 3.6: a) Reaction pathway E, b) Free energy of the species shown in (a).

3.3.5 Solvent Alkylation and the Negative Electrode SEI

Up to this point, this work has been guided by the formation of gases in LIBs. It may appear

that the work is nearly finished, since pathways have been proposed and modeled for all of

the experimentally observed species in Table 3.1. Furthermore, reaction pathway E predicts

that solid Li_2SO_3 is deposited at the negative electrode. The formation of a solid product is

consistent with previous reports that PES passivates the graphite surface.[25,59] This

prediction was further tested by preparing $LiNi_{1/3}Mn_{1/3}Co_{1/3}O_2$/graphite pouch cells with 2

wt % PES and charging the cells to 2.4 V. This cell voltage corresponds to the PES

reduction peak shown in Figure 3.4. The cell was then dissassembled under argon and the

negative electrode was taken for X-ray photoelectron spectroscopy (XPS) surface analysis.

The S 2p spectrum shown in Figure 3.7 (left panel) contains a peak that corresponds to

Li_2SO_3. The XPS spectrum also shows that at least one additional sulfur-containing species

is deposited on the graphite surface at this potential. The binding energy of this additional

peak matches the position of organic sulfonate salts (RSO$_3$Li)[84] and, perhaps, organic sulfite lithium salts (ROSO$_2$Li). Therefore, further DFT study was conducted to determine the origin of the organic sulfonate and/or organic sulfite salts in the SEI.
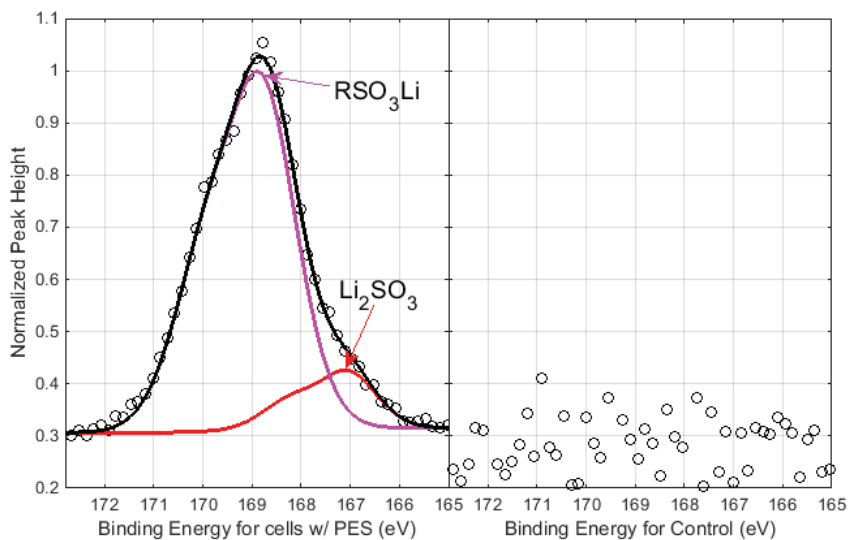
Figure 3.7: XPS spectrum of the negative electrode of 2% PES (left panel) and 0% PES (control, right panel) cells charged to 2.4 V during the first charge (see Appendix 1 for full details).

The reduced Li$_2$PES species (MS4c, shown in Figure 3.3) may be categorized as an organolithium compound. Organolithium compounds are widely used in organic chemistry as alkylating agents.[66] PES from solution or the EC and EMC solvent molecules could act as electrophiles to form C–C bonds with Li$_2$PES. Examination of the molecular geometries, valence electron configurations and and frontier orbitals (Table 3.4) reveals several possible sites for an alkylation reaction to occur. Li$_2$PES has two potential nucleophilic sites, PES has two potential electrophilic sites, EC has two potential

electrophilic sites, and EMC has three potential electrophilic sites. These reactions and their products are summarized in Table 3.5.
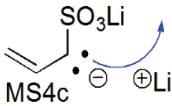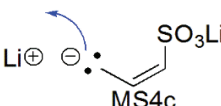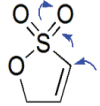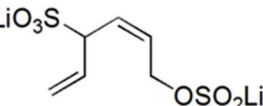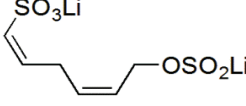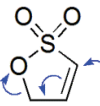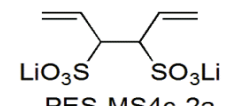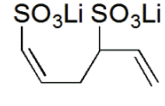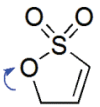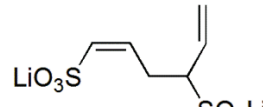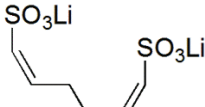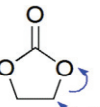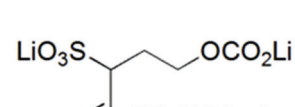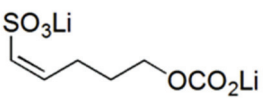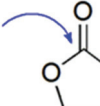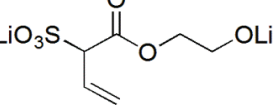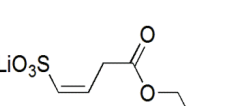
These proposed alkylation reactions are all exergonic, as shown in Figure 3.8, and the products are all organic sulfonate salts. These products are therefore consistent with the XPS spectrum in Figure 3.7 (left panel). Several of the products contain other functional groups, including sulfinite, carbonate and alkoxide salts. The electron binding energy of sulfur in sulfinite salts is not exactly known, but it is expected to be somewhere within the range of sulfonate salts and lithium sulfite. Therefore, it is impossible to know at this point whether the products include sulfinite salts. Carbonate and alkoxide salts are both commonly formed in LIBs, with or without electrolyte additives, and it would be difficult to know whether they form via the reactions in Table 3.5 or by some other route. Nevertheless, they are reasonable products to suggest.

It was considered whether any of the eighteen proposed reactions in Table 3.5 are kinetically favoured over others. On account of its resonance structures, Li_2PES has two nucleophilic sites, at the first and third carbon atoms, as shown at the top of Table 3.5. The HOMO appears fairly evenly distributed between these two sites (Table 3.4). However, the terminal carbon is perhaps the more reactive site because it is less sterically hindered. Therefore, there is a kinetic argument that the product ratio will favour those in the right column of Table 3.5 over the products in the centre column.

Table 3.4: Molecular geometries and orbital isosurfaces of Li₂PES (MS4c), PES, EC, and EMC.

	Ball-and-stick	Orbital – Front	Orbital – Side
Li₂PES (MS4c) HOMO			
PES LUMO			
EC LUMO			
EMC LUMO			

Table 3.5: Alkylation products from the reaction of Li$_2$PES (MS4c) with PES, EC, and EMC. The movement of electrons through different nucleophilic or electrophilic sites shown with blue arrows.

Electrophile	Nucleophile	
	MS4c	MS4c
EMC	EMC-MS4c-1a	EMC-MS4c-1b
EMC	EMC-MS4c-2a	EMC-MS4c-2b
EMC	EMC-MS4c-3a	EMC-MS4c-3b
EMC	EMC-MS4c-4a	EMC-MS4c-4b

62

Figure 3.8 : Gibbs free energies for the species shown in Table 5

Between the three electrophiles, PES, EC, and EMC, the relative reactivities will be governed by their concentrations and polarities. Although EMC is the most abundant, it is also the least polar (the calculated dipole moment $\mu_{EMC} = 0.66$ D). By contrast, PES is very polar ($\mu_{PES} = 6.27$ D), but typically comprises only a small fraction of the solution (e.g. 2% by weight as in Chapter 2). Therefore, EC is perhaps the most reactive electrophile because of its high concentration and its very large dipole moment ($\mu_{EC} = 7.31$ D). It is difficult to predict which electrophilic site in EC would be more reactive, since the larger LUMO isosurface suggests the carbonate carbon, whereas decreased steric hindrance and the more exergonic reaction energy favour reaction at the alkyl carbons. It is perhaps most likely that the negative electrode SEI in PES-containing cells is a mixture of the various solid products in Table 3.5.

3.3.6 Further Reduction

The species shown in Table 3.5 are products of MS4c (shown in the first row of Table 3.4) reacting with neutral solvent components. None of these products are gaseous species, consistent with the observation in Chapter 2 that PES prevents some of the gas formation

from negative electrode reactions. However, perhaps the species in Table 3.5 can be even further reduced during the first charge of Li-ion cells. If such reduction were to occur, the products should not be experimentally unobserved gaseous species. Thus, as a preliminary investigation into this matter, all EC-MS4c and PES-MS4c species (shown in Table 3.5) geometric configurations were once again optimized, but with a negative charge. EMC-MS4c species were not included in this treatment since they're likely less abundant than the other species and the computational resources were limited.

After optimization with a negative charge, some of the products were metastable as reduced species (PES-MS4c-1b, PES-MS4c-2b and PES-MS4c-3b, shown in Table 3.5, where E^0_{red}=0.39,0.41 and 0.34 vs Li/Li$^+$ respectively). For some other species (PES-MS4c-1a, PES-MS4c-2a, PES-MS4c-3a, EC-MS4c-1a and EC-MS4c-2a, shown in Table 3.5), geometry optimization calculations (relaxation) could not converge because of an $(LiSO_3)^{-1}$ departing from the original structure. $(LiSO_3)^{-1}$ would coordinate with an Li$^+$ species to form Li_2SO_3. If the full reduction step is taken as reduction, Li$^+$-coordination and Li_2SO_3 departing, all the reduction potentials are above 2.6 V vs Li/Li$^+$ for these species. The calculation for EC-MS4c-1b as an anion did not converge, but it did once an extra Li$^+$ was added to the SO$_3$Li group (E_0=0.57 vs Li/Li$^+$). The computation for EC-MS4c-2b as an anion converged, but with one negative frequency, indicating that it is perhaps a TS (E_0=0.47 vs Li/Li$^+$).

None of the species reduced into gases from these preliminary calculations, but some turned into new species with Li_2SO_3 as a by-product. Although Li_2SO_3 was observed

in the XPS spectrum shown in Figure 3.7 (left panel), the peak height is much smaller than for RSO$_3$Li. Thus, closer to the graphite surface were the conductivity is perhaps higher, reduction of the species shown in Table 3.5 is possible, for example into Li$_2$SO$_3$ and RSO$_3$Li, or, Li$_2$SO$_3$ and organo-lithium species without sulfur. However, the XPS data in Figure 3.7 (left panel) indicates that these should not be the majority constituents of the SEI due to the much stronger signal from RSO$_3$Li. Therefore, although reduction of the species shown in Table 3.5 involved potentials reached by the negative electrode, such reduction should occur for just a fraction of the species, if at all. This can perhaps be explained by a drop in electronic conductivity once an initial passivation layer is created, where afterwards reduction of the species in Table 3.5 is unlikely.

Possible further work should investigate out how the stable anions from reduction of PES-MS4c-1b, PES-MS4c-2b and PES-MS4c-3b and EC-MS4c-2a (shown in Table 3.5) should coordinate to Li$^+$ and if this agrees with the relevant XPS data. Consideration of Li$^+$-coordination may allow calculation of more accurate reduction potentials. Also, further reduction and Li$^+$-coordination should also be considered. Finally, studying the conductivity of SEI film species would be, although very difficult, very insightful.

3.4 Conclusions

In summary, carefully developed theoretical methods coupled with experimental data revealed several spontaneous pathways for the reductive decomposition of PES. Reaction pathways leading to all of the observed gas-phase PES decomposition products have been proposed. The pseudo-combustion of PES, paired with the formation of a rock-salt surface

layer at the positive electrode surface, has been presented as a possible route to the formation of carbonyl sulfide (OCS). This reactive electrode model is more plausible than the oxidative decomposition of PES because of the very high calculated potential of PES oxidation, E^0 = ~6.7 V vs Li/Li$^+$. At the negative electrode, PES reduction most likely occurs via two one-electron reduction steps, where $E^0_{red,1}$ = 0.9 V vs Li/Li$^+$ and $E^0_{red,2}$ = 4.3 V vs Li/Li$^+$. This is in agreement with a differential capacity peak at ~1.1 V vs Li/Li$^+$ that Xia et al. attributed to PES reduction.[62] The reduced species, Li$_2$PES, can decompose to form propyne, a predicted byproduct. However, the reaction energy barrier is quite large, consistent with the fact propyne has never been experimentally observed. Although a suitable pathway to the proposed product cyclopropene[60] could not be found, this species has never been experimentally observed. The reaction of Li$_2$PES with hydrogen and methyl radicals leads to propene, methylpropene, and propane, which have all been observed by GC-MS, and lithium sulfite. Finally, several alkylation reactions between nucleophilic Li$_2$PES and electrophilic PES, EC and EMC have been proposed. These reactions produce solid organic lithium sulfate salts. XPS measurements show that both lithium sulfite and organic lithium sulfate salts are SEI components on the negative electrode after PES reduction has taken place.

It is hoped that these results will not only provide new insight into the role and ultimate fate of PES in LIBs, but that they will also prove useful for developing new and improved electrolyte additives. Careful attention must be paid to the use of free energy, rather than electronic energies, and to solvation. In closing, by pairing experimental results with

computational chemistry, significant new insights and advances are possible that cannot be

achieved by theory or experiment alone.

Chapter 4: Oligomerizing Vinylene Carbonate

4.1 Introduction

The performance of Li-ion cells is largely dictated by the films formed at both the negative and positive electrodes and solvent blends often employ additives that affect these films in order to increase cycle life.[4,5,26] The most popular of all additives is vinylene carbonate (VC),[18] a cyclic carbonate similar to the widely used solvent molecule ethylene carbonate. This electrolyte additive has been shown to increase cycle life and reduce gassing of cells due to negative electrode reactions. The main VC-derived product formed on the negative electrode solid electrolyte interphase (SEI) has been suggested to be either an oligomer or polymer of vinylene carbonate.[18,30,43,85] Although such suggestions can date over a decade, no proper computational study has addressed the plausibility of this claim. Nonetheless, computational studies have been explicitly recommended for this specific issue.[85]

In 2009 Ouatani et al. synthesized a VC-derived polymer from a free radical initiator[18] and, from its XPS spectrum, compared it to the negative and positive electrodes of cells charged with VC. They found very close agreement, and thus inferred the presence of either oligomeric or polymeric VC (these terms will henceforth be used interchangeably, since the chain length is unknown). They published a second study, where the positive and negative electrodes were varied. They showed evidence for oligoVC on the graphite of graphite/Li-metal cells. Also, they provided evidence for oligoVC on the LCO ($LiCoO_2$) positive electrode of LCO/LTO ($Li_4Ti_5O_{12}$) cells where the LTO negative electrode showed an absence of the oligomer. They concluded that the oligomer was initiated independently

on both the negative and positive electrodes. Figure 4.1a shows the chemical structure of VC, where hydrogens are omitted. Figure 4.1b shows the structure that Ouatani et al. suggested for oligomeric vinylene carbonate (oligoVC).

In this chapter, formation mechanisms of this oligomer are considered through DFT calculations. First, reduction of VC to form a radical is considered, where the radical initiates oligomerization. The polymerization and copolymerization of ethene are also treated, given that ethene is present during the first charge of cells containing the solvent ethylene carbonate, as shown in Chapter 2.

Afterwards, the oligomerization of VC from a protonated VC initiator is considered, which perhaps could explain the oligoVC formed at the positive electrode. Finally, an oxidation mechanism involving polyketone formation is suggested, which may perhaps explain the CO_2 gas production seen with cells with VC (see Chapter 2).
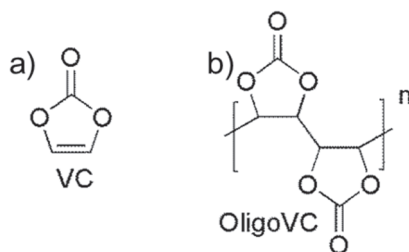
Figure 4.1: a) Vinylene carbonate molecular structure (hydrogens omitted). b) Suggested structure for oligomeric VC, or oligoVC.

The computational framework used in this chapter is the same as in Chapter 3, for which the details can be found in Appendix 1.

4.2 Radical Oligomerization of VC at the Negative Electrode

Figure 4.2 a) shows the differential capacity plot of cells with and without VC with an NMC positive electrode and graphite negative electrode. With VC (black), there is a peak at a lower full-cell voltage (2.6 V) than without VC (blue, 2.8 V). This indicates that VC is preferentially reduced over the control electrolyte. The approximate potential vs Li/Li$^+$ is shown in the top axis by subtracting the full cell voltage from 3.5 V, as in Chapter 3.
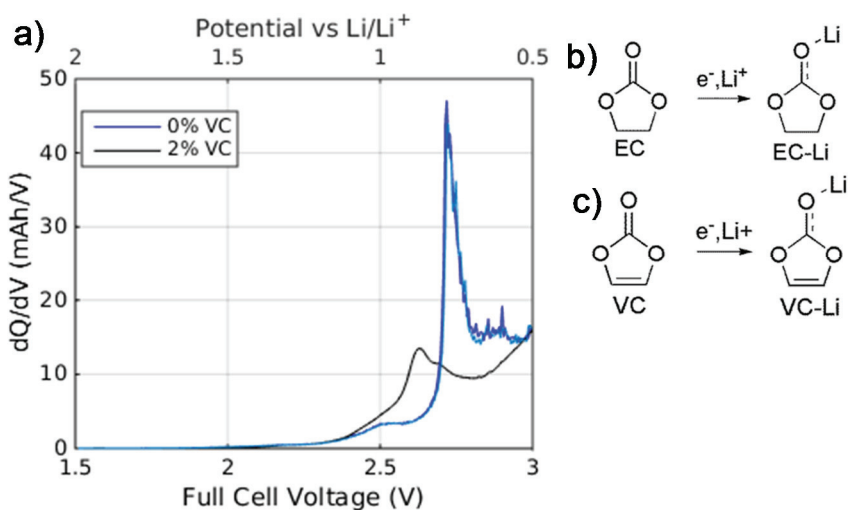
Figure 4.2: a) Differential capacity dQ/dV versus voltage during the first charge of NMC111/graphite pouch cells at 40°C for 2% VC and control (0% VC) electrolyte (data courtesy of Xia et al.).[62] b) Reduction and Li$^+$ coordination of EC. c) Reduction and Li$^+$ coordination of VC.
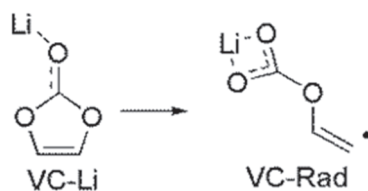
Figure 4.3: Chemical diagram of VC-Rad, originating from VC-Li.

The reduction and lithium coordination of EC, shown in Figure 4.2 b) involves a reduction potential of 0.5 V vs Li/Li$^+$ (calculated computationally). The reduction and Li$^+$-coordination of the co-solvent VC, as shown in Figure 4.2 c), is similarly 0.7 V vs Li/Li$^+$ (calculated computationally). This implies preferential reduction of VC over EC, which qualitatively agrees with Figure 4.2a.

It has been suggested or implied that the reduced VC could undergo ring opening into a radical,[18,30,39,85] as shown in Figure 4.3. The formation of the radical from the VC-Li species is energetically favourable (exergonic, as shown in Figure 4.4b), and the cis-radical is more favourable than the trans-radical (omitted here). Wang et al. in 2002, through their DFT calculations, found the formation the radical "VC-Rad" to be exergonic, albeit with a 0.9 eV energy barrier.[39] Ouatani et al. in 2008 suggested that this radical could initiate oligomerization. Unfortunately, Wang et al. only considered the reaction of the radical with other reduced VC species coordinated with Li$^+$, and not neutral VC molecules. The addition of neutral VC molecules to the VC radical "VC-Rad" is shown below in Figure 4.4a. The free energies are shown in Figure 4.4b.
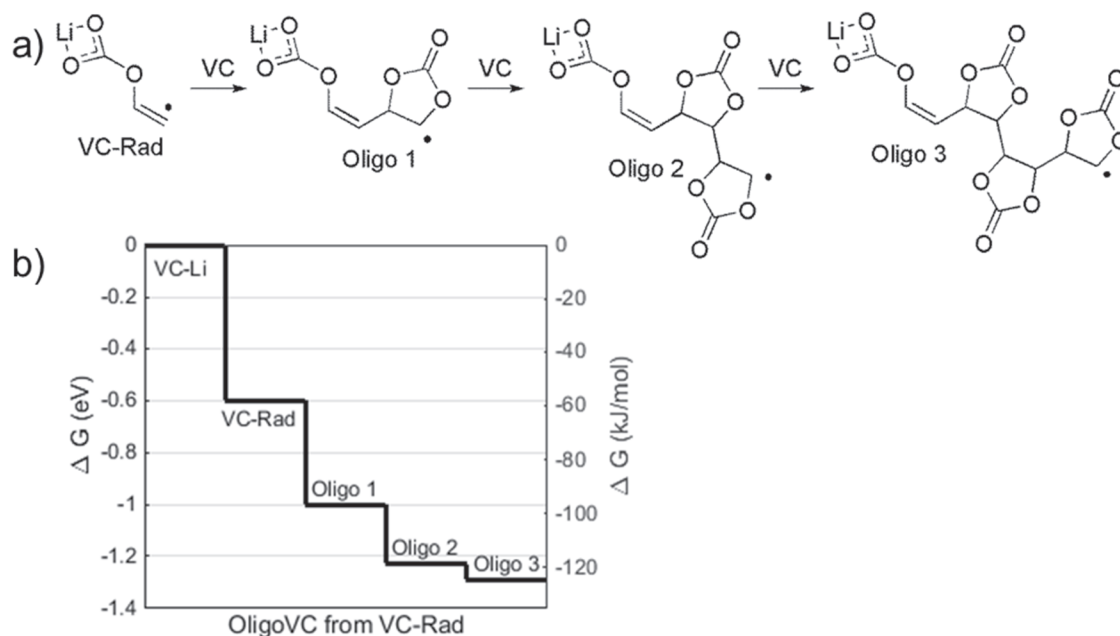
Figure 4.4: a) OligoVC formation scheme from VC-Rad. b) Gibbs free energy for the formation of the cis radical from the reduced VC-Li structure and subsequent step-wise oligomerization.

Figure 4.4b shows that the step-wise addition of neutral VC molecules to the radical initiator is favourable for the first three monomer additions. This may indicate that the oligomerization is exergonic for further monomer additions, and termination could occur with addition of another VC-Rad. Further computation, although expensive, may provide insight regarding the favourability of longer chain lengths. Although the lack of transition states may indicate that oligomerization should be instantaneous, the work here does not take into account mass-transport and diffusion, which is out of the scope of this thesis. Ding et al. synthesized polymeric VC at 50°C using a radical initiator (azobisisobutylonitrile) inside a VC solution (initiator to monomer ratio in weight of

0.015/5), and obtained 20% yield after 40 hours.[86] This may indicate that the SEI formation of oligoVC happens on the order of tens or even hundreds of hours. This is consistent with the GC-MS measurements of Petibon et al. who showed that not all VC is consumed initially during formation.[52] Petibon et al. state that "while an important portion of the initial VC present in the cell reacts early on during the [formation] charge (before the cell potential reaches 3.0 V), there is still a substantial amount of VC that reacts later on."[52]

Since formation of the VC-Rad first requires reduction of VC, the necessary voltage must be attained by the negative electrode. This would explain why LTO cells, with higher operating voltages versus Li/Li^+ than graphite, do not allow formation of oligoVC.[85] Thus, the schemes shown in Figures 4.3 and 4.4a are consistent with the absence of oligoVC inferred from Ouatani et al.'s XPS measurement on LTO negative electrodes.[85] Also, due to the preferential reduction of VC, the formation of oligoVC would explain why, with VC, there is less gas formed at the negative electrode: the VC-derived oligomer would, at least partially, passivate the negative electrode preventing some of the reduction of EC into ethylene, as explained in Chapter 1.

It has also been suggested that VC could be oligomerized through different configurations other than by attaching at the C-C double blond.[43] The LUMO diagram for VC is shown in Figure 4.5. The most pronounced lobes are on the carbons in the C-C double bond. This indicates that these are the sites are the most prone to be electrophilically attacked during monomer addition. Thus in this treatment, only VC monomer addition

through the reactive double bond C-C sites are considered. Potential further computational work should explore other configurations.
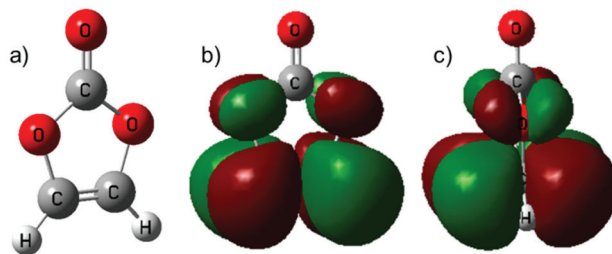
Figure 4.5 a) Vinylene carbonate (VC) ball and stick diagram. b) VC LUMO with isocontour value of 0.02. c) VC LUMO as in b), but shown by profile.

As shown in Chapter 2, there is evidence that ethene is consumed at low voltage for cells with VC. Thus it is worth evaluating whether the VC-Rad can polymerize ethene, which could explain the gas consumption feature. Figure 4.6a shows both a schematic of formation of polyethylene (PE) and a possible copolymer of both ethene and VC (PE-VC). The respective energies of PE and the copolymer are shown in Figure 4.6b and 4.6c. Both oligomers (PE and PE-VC) are exergonic for at least the first three monomer additions. The changes in free energy are consistent with the experimentally obtained free energy change for polymerization per ethene monomer at RT, which has been found to be 0.60 eV.[87] This is on the same order of magnitude as the values obtained in Figures 4.6b and 4.6c. The copolymer formation for PE-VC, as shown in Figure 4.6c, is more exergonic at the second and third monomer additions compared to ethene additions. Thus, in Li-ion cells, where there is both ethene and VC, it is likely oligomers formed on the negative electrode would not simply be oligoVC but a copolymer of both VC and ethene, given that

the concentration of both VC and ethene in the electrolyte is on the same order of magnitude. Also, Ding et al. experimentally found that vinylene carbonate can copolymerize with other organic molecules, consistent with the idea of copolymerization of VC with ethene.[88] For example, Ding et al. synthesized copolymers of VC with ethylene glycol monovinyl ether and and methyl triethylene glycol vinyl ether.[88] As seen in Chapter 2, there are ~1×10^{-4} moles of ethene in cells with 2% wt VC, while there are initially 2×10^{-4} moles of VC. It is unlikely VC-Rad would directly react with the neutral solvent components EC and EMC given that carbon bonds are saturated, however, perhaps reduction products of these species (other than ethene) could react with VC, which should be investigated in further work.

Due to the low polarity of ethene compared to VC (0.0 vs 6.1 Debye, calculated), it can be expected that chains with less polyethylene and more VC allow better Li-ion transport, and perhaps better cycle life. If a Li-ion pouch cell with a graphite negative electrode were clamped during the first charge and degassed, there should be less polymerized ethene due to the mechanical forcing of the gas outside of the electrode stack due to the clamping. Furthermore, if a cell with VC were to be held at a voltage that allows formation of the VC-Rad but doesn't allow the reduction of EC, there should be passivation of the negative graphite electrode with oligoVC without formation of as much ethene during the first charge. For example, LCO/graphite cells could be held at about 2.7 V, say for 48 hours. This is at a lower full-cell voltage than the EC reduction feature, as shown in Figure 4.1a. Both of these experiments could be carried out in further work, where coulombic efficiency could be used to compare cells formed with the different procedures.

75
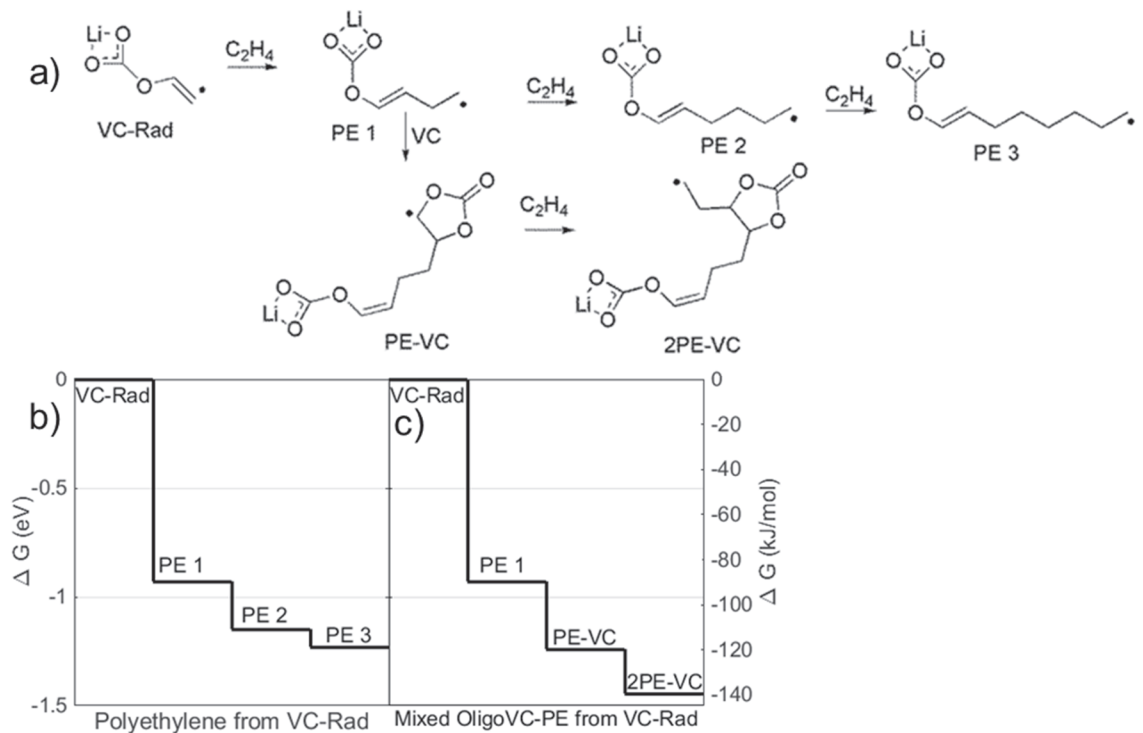
Figure 4.6: a) Scheme showing how VC-Rad, through addition of ethene, can form polyethylene (PE). Stepwise formation of a copolymer of both ethene and VC is shown (PE-VC and 2PE-VC). b) Free energies for the PE stepwise addition. c) Free energies for the PE-VC-PE stepwise addition for copolymer formation.

It may also be possible to form customized copolymer films on the graphite negative electrode by using other additives with VC. For example, if there were a second additive with a double or triple bond, co-polymerization may occur. Such an additive should also have a reduction potential at a higher full cell voltage than VC (e.g. below 0.7 vs Li/Li$^+$ according the DFT calculations in the present work) to allow formation of the VC-Rad initiator before passivation of the negative electrode. Furthermore, the additive could be cyclic, perhaps with a carbonyl or sulfonyl group, for high polarity and good Li-transport.

Candidates could be screened computationally by calculating the reduction potential, the dipole moment, and verifying that copolymerization is exergonic.

4.3 Oligomerization of VC at the Positive Electrode

Although it has been reported that the negative electrode is itself improved by addition of VC, Xiong et al. showed that for graphite/lithium cells with VC, the additive shows no significant improvement over the control electrolyte.[89] In fact, the benefits of VC were only noticeable for the positive electrode, in their case NMC.[89] Ouatani et al. suggest that "an equivalent oxidation mechanism of VC into a radical cation occurs at the positive electrode, leading finally to the same radical polymerization process, with a possible catalytic activity of the active material surface."[85] Takamatsu et al. also suggest that a VC-derived polymeric species can form at the positive electrode due to the lower oxidation potential of VC compared to EC.[90] Takamatsu et al. refer to work by Borodin et al.[76] while suggesting that VC is preferentially oxidized over EC. Although this might be true, oxidation-induced polymerization is overall a dubious suggestion due to the fact that the calculated oxidation potentials for VC are well above 5.5 V in the work by Borodin et al.[76] And so, either the calculated oxidation potentials are calculated with high error, or the polymeric species observed by Ouatani et al. before 4.2 V (full cell voltage)[18,85] on the positive electrode were not initiated by an oxidized VC molecule.

The inconsistencies underlying the proposal of cationically initiated radical polymerization at the positive electrode motivate search for an alternative form of polymerization. Protonated VC (VC+H$^+$) as an initiatior for polymerization, or oligoVC

formation, on the positive electrode is herein proposed and treated. However, as of yet, it is unclear whether any species in the electrolyte, whether by-products of film formation, or even impurities are sufficiently acidic for VC protonation.

Figure 4.7a shows a scheme where protonated VC (VC+H$^+$) can initiate formation of oligoVC. At every step, loss of a proton can terminate the chain growth, which can be restarted by proton gain. Figure 4.7b shows that every addition of VC to a protonated species represents a small energy barrier (~0.2 eV) for a more exergonic termination. In other words, after termination, the 4VC oligomer is more exergonic than 3VC, which is more exergonic than 2VC etc. Thus, although perhaps a slow process, chain growth to at least 4VC is possible. Nonetheless these energy barriers are small enough that oligomerization would be possible. Kim et al. found that the experimentally realized acid-catalyzed furfuryl alcohol oligomer formation involved activation energies similarly computed to be 0.45 eV.[91] In Figure 4.7b, the activation energies are slightly below this value, thus implying that these barriers are reasonable for oligomerization.
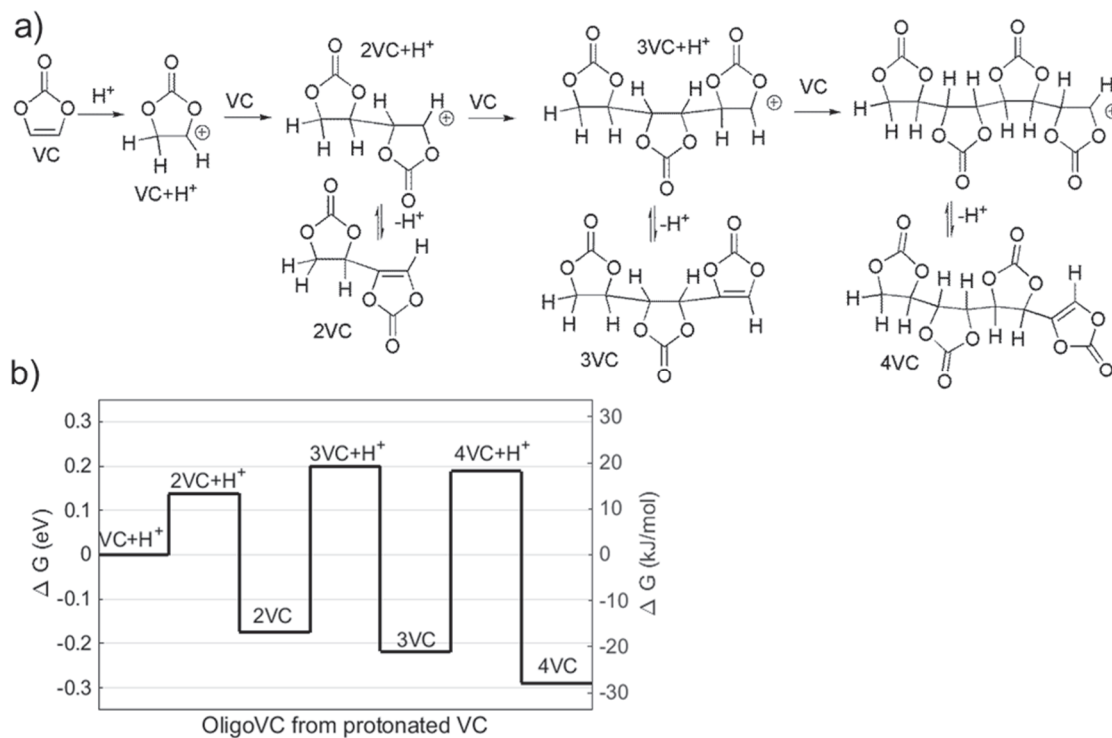
Figure 4.7: a) Scheme showing oligoVC formation from a protonated species, with termination possible through loss of the proton. b) Free energies for the structures shown in a). Free energy difference between VC and VC+H^+ is not shown due to the unknown source of H^+.
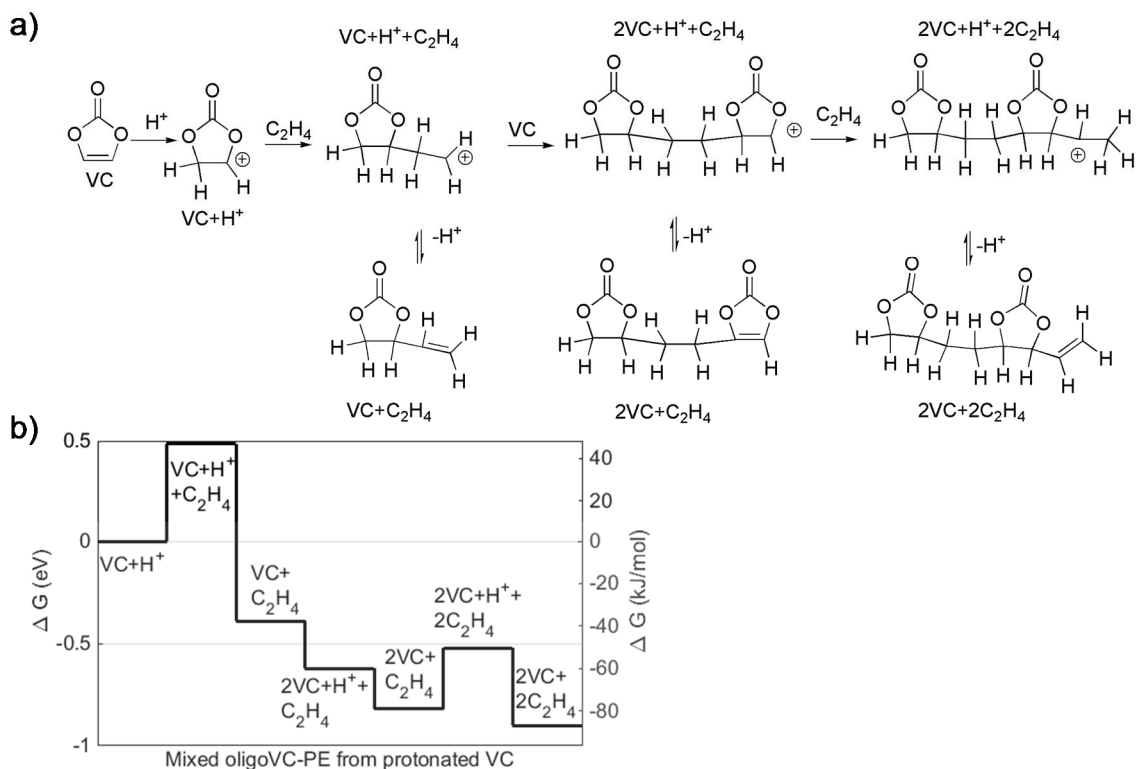
Figure 4.8: a) Scheme showing formation of a copolymer of VC and ethene from a protonated VC species (VC+H$^{+\cdot}$) b) Free energies for the structures shown in a).

Figure 4.8a shows the scheme of a copolymer of VC and ethene formed from a protonated VC species. Figure 4b shows that the copolymer, at every termination step (e.g. VC+C$_2$H$_4$, 2VC+C$_2$H$_4$ and 2VC+2C$_2$H$_4$), is even more favourable than the strictly VC chain after termination, as shown in Figure 4.7.

Figures 4.7 and 4.8 show that, provided there is a proton donor, VC oligomerization and co-polymerization with ethene is likely. Ouatani et al. have also shown absence of oligoVC in cells with a LiFePO$_4$ positive electrode,[85] indicating that the formation of the oligomer in, say an LCO positive electrode, may be surface mediated. Further work should

determine what, if any, species in electrolyte can act as proton donor to verify the plausibility the schemes shown in Figures 4.7a and Figure 4.8a. Nonetheless, once again, different additives with double or triple bonds could be tested experimentally or computationally as copolymer candidates to enhance the film on the positive electrode.

4.4 Degradation of VC at the Positive Electrode

As shown in Chapter 2, at high voltage, cells with VC produce more CO_2 than cells with control electrolyte alone. This suggests that VC can be perhaps oxidized to form CO_2. However, as stated in the previous subsection, the oxidation potential for VC is much higher than the operating cell voltage for which significant CO_2 is seen (e.g. above 4.3 V as shown in Chapter 2). Perhaps it is not the single VC molecule that is oxidized, but the film present on the positive electrode that is oxidized and degrades into CO_2. Figure 4.9a shows a scheme of oligoVC producing a polyketone and CO_2. Such a process would be consistent with both the observation of oligoVC on the positive electrode and CO_2 gas formation at high voltage. However, no conclusive evidence for polyketone formation on positive electrodes in Li-ion cells could be found in the literature.[30,92] This may indicate that either this is not the correct mechanism, that the polyketone is itself very reactive, or, that the polyketone is difficult to observe (e.g. by FTIR) due to its solubility, or the presence of other carbonyl containing species either in the electrolyte or on the positive electrode. As a, perhaps oversimplified, quantum chemistry model, the oligoVC chain has been approximated by VC attached to two R groups where R is a methyl group, as shown in Figure 4.9b.

For the neutral species, there is a transition state involving migration of a hydrogen atom (PK-neut-TS1 in Figure 4.9b) with a very high activation free energy (2 eV), as shown in Figures 4.9b and e. Although the product (PK-neut-MS2 in Figure 4.9b) has a lower free energy than the reactant (R-VC-R in Figure 4.9b), this process is not kinetically favourable due to the high activation energy. This is consistent with the stability of the film seen on the negative and positive electrodes.[18,85]

However, if oxidized, as shown in Figure 4.9c, the transition state can be formed with a much lower energy barrier (0.6 eV), as shown in Figure 4.8e. The final product PK-cat-MS2 is less exergonic compared to the oxidized structure PK-cat-MS1. The oxidation of R-VC-R involves a very high energy and potential (8.3 eV and E^0=6.9 V vs Li/Li$^+$, respectively). However, if the full oxidation step, which may be surface mediated, occurs from R-VC-R directly to PK-cat-MS2, the oxidation potential drops to 4.5 V, consistent with the potential at which CO_2 formation is noticeable (as seen in Chapter 2). The polyketone formed may have different structures than shown implied in Figure 4.9a, and two more structures are suggested in Figure 4.9d.

Due to the difficulty of computing oxidation of polymeric species, only a simplistic model was considered. Thus, experimental validation of such a mechanism would be necessary as this simple treatment is in itself insufficient. Perhaps using FTIR on cycled positive electrodes with VC electrolyte could provide evidence for the polyketone. Furthermore, if oligoVC were synthesized and added in considerable quantities to a positive electrode, this could prevent the signal from the polyketone carbonyl peak from

being buried under the peaks of the other carbonyl-containg species in the electrolyte or on the electrodes, such as EC.
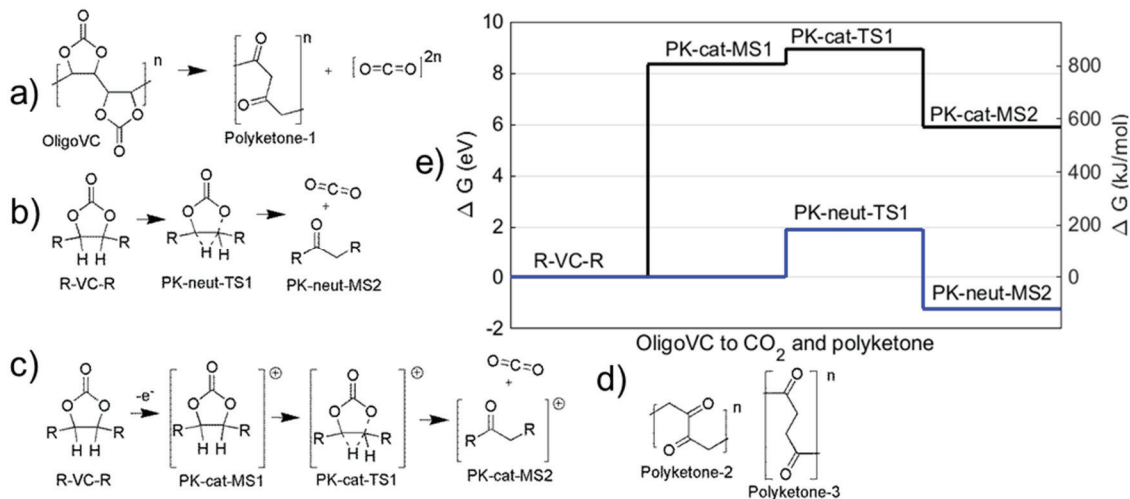
Figure 4.9 a) Scheme for OligoVC producing a polyketone. b) Scheme for neutral R-VC-R decomposing into a polyketone and CO_2. c) Scheme for R-VC-R producing a polyketone and CO_2 after oxidation. d) Different polyketone configurations. e) Free energies for schemes in b) and c).

Chapter 5: Future Work and Conclusion

5.1 Future Work

In Chapter 1, the solid electrolyte interphase (SEI) at the negative electrode in Li-ion cells and the film at the positive electrode were introduced. Generally, it can be said that one of the main tasks at hand involves understanding the film species in terms of nature, quantity and morphology, as well as the gaseous by-products. Furthermore, how agglomeration of SEI species and the morphology exactly affect electronic conductivity and lithium diffusion is still an open question. From voltage and time dependent SEI composition, electron conductivity and likeliness of electron tunneling may be quantified. Perhaps this could provide insight into whether reduction of the solvent (e.g. ethylene carbonate) or additive molecules precisely involves single or double reduction, and under which conditions (e.g. SEI thickness).

In Chapter 2, it was shown that the MAGE apparatus allowed in situ volume measurements of pouch cells. For the studied cells, it was possible to deduce that the first gas production step was largely due to negative electrode reactions while the second step was due to positive electrode reactions. It is of general interest to characterize the gas evolution of different negative and positive electrodes with different electrolyte blends. Further work is currently being undertaken to study the effect of different NMC grades with varying nickel content (e.g. NMC 111, 442 and 532 with a graphite negative electrode) on gas production.[93] GC-MS was used to identify the nature of gases formed, other than hydrogen, during the first charge. Quantifying the amount of hydrogen during the first gas

step, perhaps using a GC with a thermal conductivity detector, would be useful to confirm that the first gas is in fact mostly ethene and not hydrogen (for the same cell-drying protocol used in Chapter 2). Further work could also involve a more thorough calibration of the GC-MS (e.g. injecting known volumes of single gases one at a time and quantifying the GC-MS signal response), which would give a more precise account of the fractional composition of gases.

In Chapter 2, a gas consumption feature was observed, both between gas steps and after the second step. It was inferred from the GC-MS results that, for electrolyte with 2% VC, the gas consumption had to be at least in part ethene, provided the hydrogen amount was negligible. GC-MS measurements before, during and after consumption could provide further evidence of this. However, such measurements would be ex situ and for duplicate cells. For in situ measurements, a possible experiment would be to have sealed bags with a gas valve, for which ethene could be injected into the bag. The bag could contain individual electrodes (e.g. positive or negative electrodes in different bags), and the volume change could be monitored. Carbon dioxide, ethene and hydrogen could be injected to study possible gas consumption of these gases. Initial tests were carried out to undertake such an experiment but the sample gas bags purchased (Tedlar® Gas Sampling Bags from SigmaAldrich) leaked significant amounts of injected CO_2. Since the bags were too big to fit in a MAGE device, they had been cut up and then sealed. Thus, either the sealing process was poor, or better gas bags would have to be purchased. Such work could also confirm if ethene is the gas consumed, and on which electrode, for cells with control and 2% PES

electrolytes. This would show if ethene is the main gas being consumed in the gas consumption feature after the second gas step.

By using Henry's law and reported constants for CO_2 and C_2H_4, it was shown that the temperature dependence of gas evolution is much less pronounced than the volume change alone suggests. This is due to a drop in dissolution of gases with higher temperature. The molar quantity assessment was done approximately by assuming the first gas step involves only ethene and the second CO_2. There are, as shown in Chapter 2, other gases present, although in much smaller quantities. A more complete treatment should take into account all observed gases and their dissolution. This would however require the dependence of Henry's constants for given gases on the dissolution of other gases in the solvent. However, such a dependence has not yet been published and thus this would have to also be determined for each dissolved gases.

In Chapter 3, using quantum chemistry, exergonic pathways for the observed gases coming from the additive PES were suggested, as well as "building block" components of the negative electrode SEI. One of the gaseous pathways involved production of propene. As shown in Chapter 2, PES significantly increases the amount of propene for the first gas step. The pathway presented in Chapter 3 had Li_2SO_3 as a solid by product (pathway E, shown in Figure 3.6a), which was observed by XPS. Nonetheless, there is some propene detected for cells with the control electrolyte. Perhaps, this gas is formed by ethene swapping a hydrogen radical for a methyl radical. This would imply that EMC or EC alone as the solvents should not produce any propene, provided EMC is the source of the methyl

radicals (since we know EC is the source of ethene). Such an experiment could be carried out. Furthermore, if EMC alone did not produce any propene, then the nature of the gases formed with PES and EMC (with no EC) should be studied. If propene were present in such a case, then this would be consistent with the pathway E proposed in Chapter 3, and suggest that EMC would be the source of hydrogen radicals. It should also be checked that cells with EC and PES (with no EMC) do not show propene evolution. However, the formation charge of cells with just EMC and PES may be a failure due to poor Li^+ dissolution in EMC. Thus, perhaps other electrolyte systems, such as sulfolane with EMC,[94] could be used in this context. Once again, it would have to be verified that, say, sulfolane with EMC does not involve propene evolution.

Further work should also involve detecting the SEI "building block" species (e.g. EC-MS4c, PES-MS4c and EMC-MS4c complexes shown in Table 3.5) in order to confirm the validity of the presented pathways. One avenue could involve use of TOF-SIMS (Time of Flight Secondary Ion Mass Spectrometry)[84] on the graphite SEI from cells with the PES additive. It may also be useful to employ a voltage-hold on cells with PES at the first differential capacity peak (e.g. about 1.1 V vs Li/Li^+) for different amounts of time and afterwards use XPS on both electrodes and GC-MS for the gaseous compounds. Besides providing general information about the kinetics of passivation, this may also provide clear evidence of whether some negative electrode SEI species are soluble enough to crossover to the positive electrode. Further work should also investigate the species formed at the positive electrode at high voltage, perhaps once again by coupling XPS measurements with quantum chemistry calculations.

The reactive electrode model, which involves pseudo-combustion of the electrolyte, was also suggested as an alternative to single-molecule oxidation of PES to explain the gaseous compound OCS. Perhaps studying the gases formed in a cell using a GC-MS that can detect small amounts of oxygen (unlike the apparatus used in Chapter 2) may allow establishment of a correlation between O_2 production and electrolyte pseudo-combustion, provided some of the O_2 does not react and therefore can be detected. Perhaps the reactive electrode model can also in part explain some of the EC "oxidation" to CO_2, for which the exact mechanism is still an open problem (as mentioned in Chapter 3). However, the proposal of polymeric ethylene carbonate, as introduced in Chapter 1, should also be treated with quantum chemistry, for which, as explained in Chapter 1, decarboxylation may be the key to CO_2 formation at high voltage in Li-ion cells.

In Chapters 3 and 4, reduction potentials of EC, VC and PES were found. For EC, VC and PES the peaks were found computationally at 0.5 V, 0.7 V and 0.9 V respectively, and experimentally at 0.8 V, 0.9 V and 1.1 V. The experimental values were found approximately since no half cell (e.g. graphite vs Li-metal counter electrode) data was acquired for PES. Although the order of preferential reduction inferred from the calculated reduction potentials agrees qualitatively with experiment, there is disagreement within the first significant digit. Thus, further work could involve finding more precise reduction potentials for EC, VC and PES, by constructing half-cells with the relevant electrolyte blend (e.g. control, VC and PES) and then comparing to calculated values. The data for the reduction potential peak, obtained by differential capacity analysis, should be also acquired for other additives and/or solvents and this should be benchmarked against calculated

reduction potentials. This would provide information as to whether the methodology used in Chapters 2 and 3 involves a systematic error in the calculation of potentials or simply a random error.

In Chapter 4 the proposition of negative electrode formation of radically-initiated oligomerization of vinylene carbonate was treated using quantum chemistry. It was found that oligoVC formation was exergonically favourable for the first three monomer additions to the radical VC-Rad, while further work could determine if longer chains are thermodynamically favourable. Anyhow, it was also found that polymerization of VC would likely also occur with copolymerization of ethylene, consistent with the gas consumption feature revealed by the MAGE measurements in Chapter 2. Although a gas consumption feature after the first gas step was observed for the control electrolyte (see Figure 2.4), it was less significant than for VC, likely implying that more gas is consumed with VC. As explained in Chapter 4, further work can involve different charging, clamping and degassing protocols that would reduce the amount of ethene, perhaps allowing for better Li-transport. Namely, it may be useful to employ a voltage hold at the first differential capacity peak for around 50 h for passivation of the negative graphite electrode before EC is reduced into (among other products) ethene. Alternatively, cells can be clamped during formation and then degassed to reduce the amount of ethene dissolved in solution during the proposed oligoVC formation. Protonated-VC was also treated as a possibility for formation of oligo-VC on the positive electrode of Li-ion cells. Further work should seek to determine what species, if any, in a Li-ion cell, could provide a proton to VC. It was also suggested in Chapter 4 that different additives, e.g. with a double bond,

could be used to form copolymers with VC, provided these additives do not passivate the electrodes before polymerization is initiated. Finally, a polyketone formation mechanism was presented that may explain why cells with the VC additive produce much more CO_2 gas at high voltage than control (see Chapter 2). Possible further work for finding evidence of this mechanism was also suggested, i.e. using spectroscopy on positive electrodes into which synthesized oligo-VC is added before cell formation.

5.2 Conclusion

To conclude, this thesis used in situ volume measurement of Li-ion pouch cells coupled with quantum chemistry calculations to better understand the role of two additives: PES and VC. For PES, a newer additive, species were suggested for the negative electrode which could, at least in part, explain the characteristic role of PES in negative electrode passivation. PES was shown to be preferentially reduced during passivation of the negative electrode, and the reduction decomposition species did not involve ethene, thus explaining why less gas was produced during cell formation. For VC, oligomerization into oligoVC was shown to be favourable during passivation of the negative electrode, and perhaps also occurs on the positive electrode. Copolymerization with ethene was also shown to be likely, which agrees with a gas consumption feature observed by MAGE measurements. Finally, for VC, this leads to suggestion of different formation protocols or additive blends to customize or enhance film formation, which could be undertaken in future work.

Appendix 1

A.1 Computational Methods

A.1.1 Functional

The B3LYP hybrid functional[95] is certainly the most popular DFT functional and it generally provides excellent speed and accuracy. However, numerous other functionals have been published, several of which are available in the Gaussian09 software package. Jónsson and Johansson compared calculated vertical ionization potentials of anions using several DFT functionals, including B3LYP, and a complete basis set (CBS) extrapolation (a very accurate but time-consuming method that combines CCSD(T) and MP2 calculations).[77] The hybrid (B3LYP, M06-2X, PBE0, TPSSh) and double hybrid functionals (mPW2PLYP, B2PLYP) all performed similarly, whereas the non-hybrid functionals (VSXC, M06-L) gave poor results. Although M06-2X did give slightly more accurate values than the other methods, the improvements were deemed marginal enough that the authors did not endorse this functional over the others. Similarly, the heats of formation are comparable between various functionals.[96] Therefore, it was concluded that the use of B3LYP is preferred, since it provides comparable accuracy to other available functionals and has the benefit of allowing freer comparison with results from other researchers.

Basis Set

DFT calculations of the ionization potentials for Li-ion relevant species have been calculated using a variety of basis sets, including 6-31g(d,p),[79,97] 6-311+g(d),[77] 6-311++g(d),[98] 6-311+g(3df,2pd).[99] Of these, the higher level split-valence basis set, *i.e.* 6-311g, is becoming more common than its predecessor, *i.e.* 6-31g, as processing speeds improve.

The inclusion of diffuse functions is especially important for anions, in which the electron-electron repulsion causes the electrons to spread out more. Diffuse functions are often not used on the hydrogen atoms because of their low electron density. However, for small molecules such as those studied here, the inclusion of these additional orbitals does not add much to the computation time and allows for the possibility of high electron density hydrogen atoms.

Polarization functions may be viewed as analogous to the traditional atomic orbitals used in Hartree-Fock theory (2s, 3p, etc.) even though, strictly, DFT uses Kohn-Sham orbitals. Because the S atom in PES is hypervalent, the inclusion of d-type functions is essential to obtain good results. For the small molecules in this work, the inclusion of p-type orbitals on the H atoms is expected to improve the accuracy slightly at a minimal computational cost. It was then considered whether additional polarization functions should be included. The oxidation of PES $\rightarrow$ PES$^+$, in solution ($\varepsilon = 20$, see below) was considered. The calculated standard potentials (see below) for the 6-311++G(d,p) and 6-311++G(2df,p) basis sets were 6.69 V vs. Li/Li$^+$ and 6.64 V, respectively. Although the

latter is expected to be slightly more accurate, this difference was considered negligible because the precision of experimentally measured oxidation and reduction potentials is ±0.1 V. Yet the latter basis set has considerably longer calculation times. This would have posed a major obstacle for this work because of the dozens of molecular geometry optimizations, transition state optimizations, and intrinsic reaction coordinate calculations. Therefore, the 6-311++G(d,p) was chosen to provide a good balance between computational accuracy and cost.

Solvation Model

Solute-solvent modeling is not simple and remains an area of considerable theoretical research. In order to properly represent solvent packing, one must calculate the energies for a very large number of possible geometries/configurations and then find the statistical average. Clearly, this is impractical for applied DFT studies. For example, this is a large issue in biochemical research because conformational changes of macromolecules can have great physiological significance (*e.g.*, enzymes). The polarizable continuum model (PCM) comes standard with commercial QC software.[100] This is a simple yet robust model that represents solvents by their dielectric constant (ε). The default version of this model within Gaussian09 uses the integral equation formalism variant and a universal force field to define the solvation cavity (IEFPCM-UFF).[70] Despite its simplicity, this method does an excellent job of modelling solvation effects for geometry and energy calculations, provided an accurate dielectric constant is known.[100,101] Dielectric constants for ethylene carbonate (EC)/ethylmethyl carbonate (EMC) solvent blends at various temperatures, albeit without salt, have recently been measured.[71] Because most experimental data is available for PES dissolved in 1M $LiPF_6$

3:7 EC/EMC, the value $\varepsilon = 20$ was adopted,[71] which should be a good representation of this solvent blend at room temperature ($20 \leq T \leq 25$ °C). The purpose of using a continuum model, such as PCM, is to represent the dynamic nature of solvation without the need for extensive computation. However, there are more complex methods that may be used, including COSMO, ONIOM, and hybrid cluster/continuum models. Due to its simplicity, PCM was the solvation model employed in this thesis.

A.1.2 Standard Electrode Potentials

Standard potentials may be determined using computational methods by calculating the free energy (G^0) of the reduced and oxidized species. It is by now well established that the energy of the electrons in the external circuit (i.e., in the copper or aluminium wire) does not affect the electrochemical potential.[102] Previously, the free energy of each chemical species was approximated as the sum of the gas-phase electronic energy [$E_{elec}(gas)$], the gas-phase thermal energy [$\delta G^0_{th}(gas)$], and the solvation energy (δG^0_{solv}):[79]

$$G° = E_{elec}(gas) + \delta G^0_{th}(gas) + \delta G^0_{solv} \qquad \textbf{(1)}$$

This approach has been used to calculate oxidation potentials of redox shuttles,[97,103] electrolyte additives (e.g., trimethyl phosphite[104]) and solvents.[99] In Gaussian09, however, it is much simpler to directly calculate the equilibrium electronic and thermal energies of a species in solution [$E_{elec}(sol)$ and $\delta G^0_{th}(sol)$, respectively], which reduces the sum to two terms:

$$G° = E_{elec}(sol) + \delta G^0_{th}(sol) \qquad \textbf{(2)}$$

Once these terms are determined for the reduced and oxidized species, the standard potential (E^0) may be calculated as a function of the free energy change:[105]

$$E^\circ = \frac{-\Delta G^\circ}{nF} - E_{ref} \qquad \textbf{(3)}$$

In this equation, n is the number of electrons, F is Faraday's constant, and the E_{ref} is a constant that accounts for the free energy change of the reference electrode. The exact value of this constant will depend on the properties of the electrolyte solution, because of changes in the free energy of the solvated Li^+ cation.[76] This value may then be obtained by subdividing the question into three factors, 1) the absolute potential of the standard hydrogen electrode (SHE), 2) the potential of the standard lithium electrode (SLE), in aqueous solution, relative to the SHE, and 3) the difference in the solvation energy of a Li^+ cation in water and in the Li-ion cell. Then the exact value of the reference electrode potential may be calculated:

$$E_{ref} = E^0_{SHE}(abs) + E^0_{SLE}(rel) + \frac{d(\Delta G_{solv})}{F} \qquad \textbf{(4)}$$

The absolute potential of the SHE was reported by IUPAC as 4.42 – 4.44 V. More recently, Isse and Gennaro reported the value 4.281 V.[106] The authors report that their value should provide a better estimate for use with computed absolute potentials, as is the case here. Therefore, this updated value shall be used for the calculations herein. Since it is unclear which value is the most accurate, the error on calculated reduction potentials should not be taken as less than 0.1 V. Anyhow, from preliminary calculations, it seems that there is a typical error of about 0.2 V. The second value, $E^0_{SLE,}$ is more easily measured and

reported as E^0_{SLE} = -3.04 V_{SHE}.[107] The final value may be estimated by calculating the solvation energy of a Li^+ cation in water and in solutions of various polarity, as defined by their dielectric constants. Using B3LYP/6-311++G(d,p), that the absolute potential of the Li/Li^+ electrode in our system (ε = 20) is found to be 1.44 V. This value for E_{ref} is a good match with those used in similar studies (typically ~1.4 V).[76] Therefore, E_{ref} = 1.44 V was used with equation (3) for all the standard potentials reported in this work.

A.1.3 Molecular geometries, energies and frequencies

Certain computations were computed by revision A of Gaussian on local computers, although most were computed by revision D on a remote computer cluster. The differences attributable to the different revisions of Gaussian are judged to be negligible. Unless otherwise indicated, the 6-311++(d,p) basis set was used with the B3LYP functional and the IEFPCM-UFF solvation model, where the dielectric constant was set to 20 (ε =20). All stable and metastable geometries were subject to vibrational mode analysis to confirm there are only positive frequencies . Transition state geometries all had one negative (imaginary) frequency. The thermal contributions to the free energy were all calculated at 298.15 K.
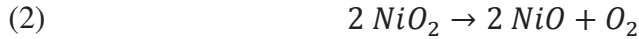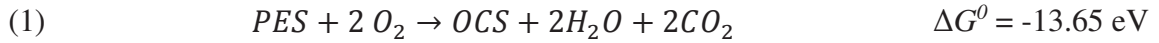
A.1.4 Oxidation

The oxidation potential of the PES molecule was calculated first. However the value obtained was quite high so different methods were considered. A functional different than B3LYP was tested. PF_6^- anions from the electrolyte salt were also explicitly included as they may decrease calculated oxidation potentials. However, the standard potential

calculated with the M06-2X functional, 7.07 V, was actually 0.38 V greater than the B3LYP value. Moreover, when PF6⁻ was included, using B3LYP, the calculated potential only decreased from the original value by 0.12 V, to 6.58 V. In all cases mentioned here, the calculated oxidation potentials were much higher than the operating cell voltage.

A.1.5 PES Pseudo-combustion

For the reactive electrode model, the free energy of PES pseudo-combustion was calculated by utilizing the state function property of the Gibbs energy, G. Therefore, the overall reaction may be divided into the decomposition of the metal oxide, followed by PES combustion.

(1) $\qquad PES + 2\,O_2 \rightarrow OCS + 2H_2O + 2CO_2 \qquad \Delta G^0 = \text{-}13.65\ \text{eV}$

(2) $\qquad 2\,NiO_2 \rightarrow 2\,NiO + O_2$

The free energy of Reaction (1) was calculated using B3LYP/6-311++g(d,p) and the IEFPCM-UFF solvation model ($\varepsilon = 20$). Reaction (2) is a 4-electron redox process. Therefore, published electrochemical data[108,109] may be used to estimate the free energy of reaction (2). The standard potential for the reduction of NiO_2 may be estimated using the reactions published by Pourbaix:[109]

(2a) $\qquad 2\,NiO_2 + 2\,H^+ + 2\,e^- \rightleftharpoons Ni_2O_3 + H_2O \qquad E^0 = 1.434\ \text{V}_{\text{RHE}}$

(2b) $\qquad Ni_2O_3 + 2\,H^+ + 2\,e^- \rightleftharpoons 2\,NiO + H_2O \qquad E^0 = 1.020\ \text{V}_{\text{RHE}}$

(2c) $\qquad NiO_2 + 2\,H^+ + 2\,e^- \rightleftharpoons NiO + H_2O \qquad E^0 = 1.227\ \text{V}_{\text{RHE}}$
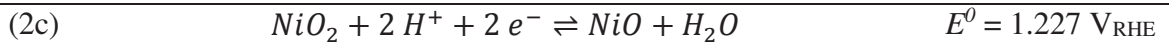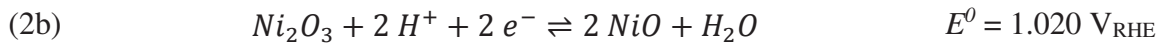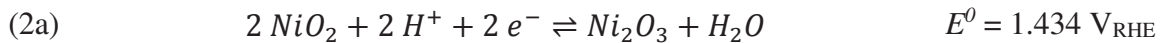
Alternatively, the standard potential for the reduction of NiO_2 may be estimated using the reactions published by Asselin *et al.*:[108]

(2d)	$2\ NiO_2 + H^+ + 2\ e^- \rightleftharpoons HNiO_2^-$	$E^0 = 0.66\ V_{RHE}$
(2e)	$HNiO_2^- + 3\ H^+ + 2\ e^- \rightleftharpoons Ni + 3\ H_2O$	$E^0 = 0.68\ V_{RHE}$
(2f)	$Ni + H_2O \rightleftharpoons NiO + 2\ H^+ + 2\ e^-$	$E^0 = 0.13\ V_{RHE}$
(2c)	$NiO_2 + 2\ H^+ + 2\ e^- \rightleftharpoons NiO + H_2O$	$E^0 = 1.21\ V_{RHE}$
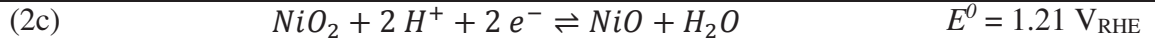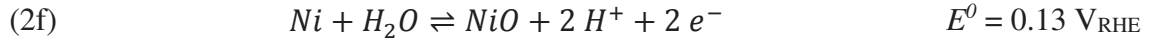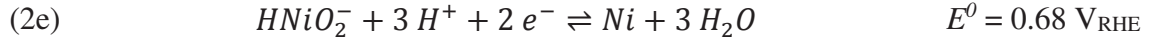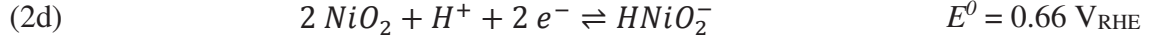
There is a small difference in the standard potential for Reaction (2c). Moreover, nickel oxides are extremely prone to hydration disorder and rapidly form nickel hydroxides/oxyhydroxides in aqueous media.[109–111] The standard electrode potentials used for this estimate were all measured in aqueous electrochemical experiments and, hence, there is inherent error in these values. Nevertheless, this error is unlikely to be much more than ± 0.1 V, which will be shown to be quite acceptable for the final result below. The oxidation process in Reaction (2) is simply the formation of oxygen:

(2g)	$2H_2O \rightleftharpoons O_2 + 4\ H^+ + 4\ e^-$	$E^0 = 1.229\ V_{RHE}$
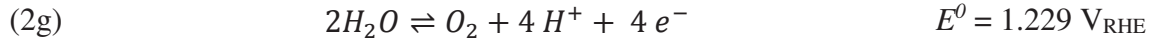
The standard free energy of Reaction (2) was then calculated by combining Reaction (2c) and (2g), using $\Delta G^0 = -nFE^0$, $n = 4$:

(2)	$2\ NiO_2 \rightarrow 2\ NiO + O_2$	$0.01\ eV \le \Delta G^0 \le 0.08\ eV$
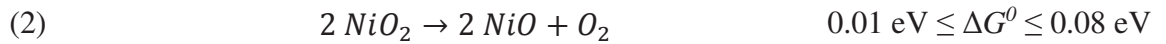
The upper value, $\Delta G^0 = 0.08$ eV, was used to conservatively estimate the overall energy of PES pseudo-combustion (3):

(3)	$2\ NiO_2 + PES \rightarrow 2\ NiO + OCS + 2H_2O + 2CO_2$	$\Delta G^0 \le -13.57\ eV$
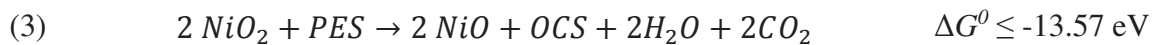
A.2 Cell Preparation for XPS

Machine made 220 mAh $LiNi_{1/3}Mn_{1/3}Co_{1/3}O_2$/graphite pouch cells balanced for 4.2 V operation were obtained dry (vacuum sealed with no electrolyte) from Li-Fun Technology (Xinma Industry Zone, Golden Dragon Road, Tianyuan District, Zhuzhou City, Hunan Province, PRC, 412000). Two identical pouch cells were prepared for reproducibility. After heating to 80°C under vacuum for 12 h to remove any residual water, the pouch cells were filled with 0.9 g of electrolyte in an argon-filled glove box. The electrolyte was 1 M $LiPF_6$ (BASF, purity 99.94, water content 14 ppm) EC:EMC (3:7 by weight, BASF, water content less than 20 ppm) with 2 wt % PES (Lianchuang Medicinal Chemistry Co., > 98.20%) or without ("control" cells). Cells were vacuum-sealed at -94 kPa (relative to atmospheric pressure) using a compact vacuum sealer (MSK-115A, MTI Corp.).

After filling, formation was performed on a Maccor 4000 series cycler as follows. Cells were placed in a temperature-controlled box at 40.0 ± 0.1°C and held at 1.5 V for 24 h to allow for the completion of wetting. Cells were charged to either 2.4 V or 3.5 V at a current of 11 mA (C/20) then the voltage was held until the measured current decreased to 0.005C so that electrodes were in electrochemical equilibrium. Pouch cells were then carefully disassembled in an argon-filled glove box. Electrodes were then cut from the pouch cells electrodes with a precision punch and washed twice by immersion into 0.8 mL of EMC solvent (BASF) in a clean and dry glass vial with a mild manual agitation for 10 s to remove the majority of the $LiPF_6$ salt.

For the dQ/dV vs. V analysis, the graphite potential was estimated as follows: High-precision reference potential-specific capacity data for Li/graphite and Li/LiNi$_{1/3}$Mn$_{1/3}$Co$_{1/3}$O$_2$ electrodes as well as the full LiNi$_{1/3}$Mn$_{1/3}$Co$_{1/3}$O$_2$/graphite pouch cell potential-specific capacity data were first recorded. Then, from these data, the dV/dQ vs. Q of a LiNi$_{1/3}$Mn$_{1/3}$Co$_{1/3}$O$_2$/graphite pouch cell was calculated and compared to the experimental curve using a differential potential analysis software previously developed at Dalhousie University[112] which suppresses the need for a reference electrode to obtain the anode potential versus lithium metal.

A.3 X-ray Photoelectron Spectroscopy (XPS)

XPS was performed on a SPECS spectrometer equipped with a Phoibos 150 hemispherical energy analyzer and using Mg Kα radiation (hv = 1253.6 eV). To transfer air-sensitive samples from the argon-filled glove box to the spectrometer, a special transfer system was used as described in reference "Madec et al.".[35] Shortly, samples were mounted onto a molybdenum holder using a copper conductive tape (3M) and placed into the transfer system under argon. The later was put under vacuum at approx. 10^{-3} mbar for 1 h and then connected to the spectrometer where samples were loaded under a pressure of ~10^{-3} mbar. All samples were kept at 10^{-8} mbar for one night before analysis to allow a strictly identical vacuum procedure.

The analyzed sample area was ~ 2 x 3 mm^2 which gives results representative of the whole electrode. Core spectra were recorded in the fixed analyser transmission (FAT) mode with a 20 eV pass energy at an operating pressure < 2 x 10^{-9} mbar. Short acquisition time spectra were first recorded as reference to follow any possible sample degradation

during the analysis. Data treatment was performed using CasaXPS software. The binding energy scale was calibrated from the C1s peak at 285 eV (C-C/C-H) for the graphite electrodes analyzed here. Nonlinear Shirley-type background[113] was used for core peaks analysis while 70% Gaussian - 30% Lorentzian Voigt peak shapes and full width at half-maximum (fwhm) constraint ranges were selected to optimized areas and peak positions.

References

(1)   Levine, S. *The Powerhouse: Inside the Invention of a Battery to Save the World*;
        Viking, 2015.

(2)   Burns, J. C.; Kassam, A.; Sinha, N. N.; Downie, L. E.; Solnickova, L.; Way, B.
        M.; Dahn, J. R. *J. Electrochem. Soc.* **2013**, *160* (9), A1451.

(3)   Reddy, J. *Linden's Handbook of Batteries*, Fourth Edition.; McGraw-Hill, 2011.

(4)   Xu, K. *Chem. Rev.* **2004**, *104* (10), 4303.

(5)   Xu, K. *Chem. Rev.* **2014**, *114* (23), 11503.

(6)   Aurbach, D. *Nonaqueous Electrochemistry*; Marcel Dekker, 1999.

(7)   Ding, M. S.; Xu, K.; Jow, T. R. *J. Electrochem. Soc.* **2000**, *147* (5), 1688.

(8)   Ding, M. S.; Xu, K.; Zhang, S. S.; Amine, K.; Henriksen, G. L.; Jow, T. R. *J.
        Electrochem. Soc.* **2001**, *148* (10), A1196.

(9)   Ding, M. S.; Xu, K.; Zhang, S.; Jow, T. R. *J. Electrochem. Soc.* **2001**, *148* (4),
        A299.

(10)   Fong, R.; von Sacken, U.; Dahn, J. R. *J. Electrochem. Soc.* **1990**, *137* (7), 2009.

(11)   Peled, E.; Golodnitsky, D.; Ardel, G. *J. Electrochem. Soc.* **1997**, *144* (8), L208.

(12)   Verma, P.; Maire, P.; Novák, P. *Electrochimica Acta* **2010**, *55* (22), 6332.

(13)   Zhuang, G. V.; Xu, K.; Yang, H.; Jow, T. R.; Ross, P. N. *J. Phys. Chem. B* **2005**,
        109 (37), 17567.

(14)   Nie, M.; Chalasani, D.; Abraham, D. P.; Chen, Y.; Bose, A.; Lucht, B. L. *J. Phys.
        Chem. C* **2013**, *117* (3), 1257.

(15)   Wang, Y.; Nakamura, S.; Ue, M.; Balbuena, P. B. *J. Am. Chem. Soc.* **2001**, *123*
        (47), 11708.

(16)   Aurbach, D.; Markovsky, B.; Weissman, I.; Levi, E.; Ein-Eli, Y. *Electrochimica
        Acta* **1999**, *45* (1), 67.

(17)   Aurbach, D.; Levi, M. D.; Levi, E.; Schechter, A. *J. Phys. Chem. B* **1997**, *101* (12), 2195.

(18)   El Ouatani, L.; Dedryvère, R.; Siret, C.; Biensan, P.; Reynaud, S.; Iratçabal, P.; Gonbeau, D. *J. Electrochem. Soc.* **2009**, *156* (2), A103.

(19)   Yang, L.; Ravdel, B.; Lucht, B. L. *Electrochem. Solid-State Lett.* **2010**, *13* (8), A95.

(20)   Arthur, C. *The Guardian*. October 17, 2013,.

(21)   Markovsky, B.; Levi, M. D.; Aurbach, D. *Electrochimica Acta* **1998**, *43* (16), 2287.

(22)   Obrovac, M. N.; Christensen, L.; Le, D. B.; Dahn, J. R. *J. Electrochem. Soc.* **2007**, *154* (9), A849.

(23)   Aiken, C. P.; Xia, J.; Wang, D. Y.; Stevens, D. A.; Trussler, S.; Dahn, J. R. *J. Electrochem. Soc.* **2014**, *161* (10), A1548.

(24)   Berkes, B. B.; Jozwiuk, A.; Vračar, M.; Sommer, H.; Brezesinski, T.; Janek, J. *Anal. Chem.* **2015**, *87* (12), 5878.

(25)   Li, B.; Wang, Y.; Rong, H.; Wang, Y.; Liu, J.; Xing, L.; Xu, M.; Li, W. *J. Mater. Chem. A* **2013**, *1* (41), 12954.

(26)   Wang, D. Y.; Xia, J.; Ma, L.; Nelson, K. J.; Harlow, J. E.; Xiong, D.; Downie, L. E.; Petibon, R.; Burns, J. C.; Xiao, A.; others. *J. Electrochem. Soc.* **2014**, *161* (12), A1818.

(27)   Hartmann, P.; Grübl, D.; Sommer, H.; Janek, J.; Bessler, W. G.; Adelhelm, P. *J. Phys. Chem. C* **2014**, *118* (3), 1461.

(28)   Castel, E.; Berg, E. J.; Kazzi, M. El; Novák, P.; Villevieille, C. *Chem. Mater.* **2014**, *26* (17), 5051.

(29)   Novák, P.; Goers, D.; Hardwick, L.; Holzapfel, M.; Scheifele, W.; Ufheil, J.; Würsig, A. *J. Power Sources* **2005**, *146* (1-2), 15.

(30)   Zhang, B.; Metzger, M.; Solchenbach, S.; Payne, M.; Meini, S.; Gasteiger, H. A.; Garsuch, A.; Lucht, B. L. *J. Phys. Chem. C* **2015**, 150512180451000.

(31)   He, M.; Castel, E.; Laumann, A.; Nuspl, G.; Novák, P.; Berg, E. J. *J. Electrochem. Soc.* **2015**, *162* (6), A870.

(32)   Dahn, J. R.; Trussler, S.; Dugas, S.; Coyle, D. J.; Dahn, J. J.; Burns, J. C. *J. Electrochem. Soc.* **2013**, *160* (2), A251.

(33)   Self, J.; Aiken, C. P.; Petibon, R.; Dahn, J. R. *J. Electrochem. Soc.* **2015**, *162* (6), A796.

(34)   Aurbach, D. *J Power Sources* **1999**, *89*, 206.

(35)   Madec, L.; Xia, J.; Petibon, R.; Nelson, K. J.; Sun, J.-P.; Hill, I. G.; Dahn, J. R. *J. Phys. Chem. C* **2014**, *118* (51), 29608.

(36)   Aurbach, D.; Ein-Ely, Y.; Zaban, A. *J. Electrochem. Soc.* **1994**, *141* (1), L1.

(37)   Broussely, M.; Biensan, P.; Bonhomme, F.; Blanchard, P.; Herreyre, S.; Nechev, K.; Staniewicz, R. J. *J. Power Sources* **2005**, *146* (1-2), 90.

(38)   Sinha, N. N.; Smith, A. J.; Burns, J. C.; Jain, G.; Eberman, K. W.; Scott, E.; Gardner, J. P.; Dahn, J. R. *J. Electrochem. Soc.* **2011**, *158* (11), A1194.

(39)   Wang, Y.; Nakamura, S.; Tasaki, K.; Balbuena, P. B. *J. Am. Chem. Soc.* **2002**, *124* (16), 4408.

(40)   Xing, L.; Li, W.; Wang, C.; Gu, F.; Xu, M.; Tan, C.; Yi, J. *J. Phys. Chem. B* **2009**, *113* (52), 16596.

(41)   Xing, L.; Borodin, O. *Phys. Chem. Chem. Phys.* **2012**, *14* (37), 12838.

(42)   Onuki, M.; Kinoshita, S.; Sakata, Y.; Yanagidate, M.; Otake, Y.; Ue, M.; Deguchi, M. *J. Electrochem. Soc.* **2008**, *155* (11), A794.

(43)   Ota, H.; Sakata, Y.; Inoue, A.; Yamaguchi, S. *J. Electrochem. Soc.* **2004**, *151* (10), A1659.

(44)   Marks, T.; Trussler, S.; Smith, A. J.; Xiong, D.; Dahn, J. R. *J. Electrochem. Soc.* **2011**, *158* (1), A51.

(45)   Metzger, M.; Marino, C.; Sicklinger, J.; Haering, D.; Gasteiger, H. A. *J. Electrochem. Soc.* **2015**, *162* (7), A1123.

(46)   Andersson, A. M.; Edström, K. *J. Electrochem. Soc.* **2001**, *148* (10), A1100.

(47)   Sloop, S. E.; Kerr, J. B.; Kinoshita, K. *J. Power Sources* **2003**, *119-121*, 330.

(48)   Gui, X.; Tang, Z.; Fei, W. *J. Chem. Eng. Data* **2010**, *55* (9), 3736.

(49)   Dougassa, Y. R.; Tessier, C.; Ouatani, L. El; Anouti, M.; Jacquemin, J. *J. Chem. Thermodyn.* **2013**, *61*, 32.

(50)   Anouti, M.; Dougassa, Y. R.; Tessier, C.; Ouatani, L. El; Jacquemin, J. *J. Chem. Thermodyn.* **2012**, *50*, 71.

(51)   NIST Webbook. NIST 2011,.

(52)   Petibon, R.; Rotermund, L.; Nelson, K. J.; Gozdz, A. S.; Xia, J.; Dahn, J. R. *J. Electrochem. Soc.* **2014**, *161* (6), A1167.

(53)   Dougassa, Y. R. Propriétés de transport et Solubilité des gaz dans les électrolytes pour les batteries lithium-ion. PhD Thesis, Université François-Rabelais de Tours, 2014.

(54)   Svens, P.; Kjell, M.; Tengstedt, C.; Flodberg, G.; Lindbergh, G. *Energies* **2013**, *6* (1), 400.

(55)   McKeen, L. W.; Massey, K. L. *Permeability properties of plastics and elastomers*; Elsevier, 2012.

(56)   Haynes, W. M. *CRC Handbook of Chemistry and Physics*, 91st ed.; 2010.

(57)   Jansen, A. N.; Amine, K.; Henriksen, G. L. *Low-cost flexible packaging for high-power Li-Ion HEV batteries.*; ANL-04/09, 828774; 2004.

(58)   Li, B.; Xu, M.; Li, T.; Li, W.; Hu, S. *Electrochem. Commun.* **2012**, *17*, 92.

(59)   Li, B.; Xu, M.; Li, B.; Liu, Y.; Yang, L.; Li, W.; Hu, S. *Electrochimica Acta* **2013**, *105*, 1.

(60)   Li, B.; Wang, Y.; Tu, W.; Wang, Z.; Xu, M.; Xing, L.; Li, W. *Electrochimica Acta* **2014**, *147*, 636.

(61)   Nelson, K. J.; Xia, J.; Dahn, J. R. *J. Electrochem. Soc.* **2014**, *161* (12), A1884.

(62)   Xia, J.; Ma, L.; Aiken, C. P.; Nelson, K. J.; Chen, L. P.; Dahn, J. R. *J. Electrochem. Soc.* **2014**, *161* (10), A1634.

(63)   Ma, L.; Xia, J.; Dahn, J. R. *J. Electrochem. Soc.* **2014**, *161* (14), A2250.

(64)   Ma, L.; Xia, J.; Dahn, J. R. *J. Electrochem. Soc.* **2015**, *162* (7), A1170.

(65)   Leslie J. Pinnell, Christopher Campion, Antoni S. Gozdz, Jeong Ju CHO. Electrolyte formulation for reduced gassing wide temperature range cycling. US20150064549 A1.

(66)   Clayden, J.; Greeves, N.; Warren, S.; Wothers, P. *Organic Chemistry*; Oxford University Press, 2000.

(67)   Becke, A. D. *J. Chem. Phys.* **1993**, *98* (7), 5648.

(68)   Cossi, M.; Rega, N.; Scalmani, G.; Barone, V. *J. Comput. Chem.* **2003**, *24* (6), 669.

(69)   Ditchfield, R.; Hehre, W. J.; Pople, J. A. *J. Chem. Phys.* **1971**, *54* (2), 724.

(70)   Frisch, M. J.; Trucks, G. W.; Schlegel, H. B.; Scuseria, G. E.; Robb, M. A.; Cheeseman, J. R.; Scalmani, G.; Barone, V.; Mennucci, B.; Petersson, G. A.; Nakatsuji, H.; Caricato, M.; Li, X.; Hratchian, H. P.; Izmaylov, A. F.; Bloino, J.; Zheng, G.; Sonnenberg, J. L.; Hada, M.; Ehara, M.; Toyota, K.; Fukuda, R.; Hasegawa, J.; Ishida, M.; Nakajima, T.; Honda, Y.; Kitao, O.; Nakai, H.; Vreven, T.; Montgomery Jr., J. A.; Peralta, J. E.; Ogliaro, F.; Bearpark, M. J.; Heyd, J.; Brothers, E. N.; Kudin, K. N.; Staroverov, V. N.; Kobayashi, R.; Normand, J.; Raghavachari, K.; Rendell, A. P.; Burant, J. C.; Iyengar, S. S.; Tomasi, J.; Cossi, M.; Rega, N.; Millam, N. J.; Klene, M.; Knox, J. E.; Cross, J. B.; Bakken, V.; Adamo, C.; Jaramillo, J.; Gomperts, R.; Stratmann, R. E.; Yazyev, O.; Austin, A. J.; Cammi, R.; Pomelli, C.; Ochterski, J. W.; Martin, R. L.; Morokuma, K.; Zakrzewski, V. G.; Voth, G. A.; Salvador, P.; Dannenberg, J. J.; Dapprich, S.; Daniels, A. D.; Farkas, Ö.; Foresman, J. B.; Ortiz, J. V.; Cioslowski, J.; Fox, D. J. *Gaussian 09*; Gaussian, Inc.: Wallingford, CT, USA, 2009.

(71)   Hall, D. S.; Self, J.; Dahn, J. R. *Submitted to J. Phys. Chem. C* **2015**.

(72)   Harris, J. *Langmuir* **1991**, *7* (11), 2528.

(73)   Guimond, N.; MacDonald, M. J.; Lemieux, V.; Beauchemin, A. M. *J. Am. Chem. Soc.* **2012**, *134* (40), 16571.

(74)   Xing, L.; Li, W.; Xu, M.; Li, T.; Zhou, L. *J. Power Sources* **2011**, *196* (16), 7044.

(75)   Zhang, S. .; Jow, T. .; Amine, K.; Henriksen, G. . *J. Power Sources* **2002**, *107* (1), 18.

(76)   Borodin, O.; Behl, W.; Jow, T. R. *J. Phys. Chem. C* **2013**, *117* (17), 8661.

(77)   Jónsson, E.; Johansson, P. *Phys. Chem. Chem. Phys.* **2015**, *17* (5), 3697.

(78)   Moshkovich, M.; Cojocaru, M.; Gottlieb, H. E.; Aurbach, D. *J. Electroanal. Chem.* **2001**, *497* (1-2), 84.

(79)   Wang, R. L.; Buhrmester, C.; Dahn, J. R. *J. Electrochem. Soc.* **2006**, *153* (2), A445.

(80)   Zheng, S.; Huang, R.; Makimura, Y.; Ukyo, Y.; Fisher, C. A.; Hirayama, T.; Ikuhara, Y. *J. Electrochem. Soc.* **2011**, *158* (4), A357.

(81)   Muto, S.; Sasano, Y.; Tatsumi, K.; Sasaki, T.; Horibuchi, K.; Takeuchi, Y.; Ukyo, Y. *J. Electrochem. Soc.* **2009**, *156* (5), A371.

(82)   Makimura, Y.; Zheng, S.; Ikuhara, Y.; Ukyo, Y. *J. Electrochem. Soc.* **2012**, *157* (7), A1070.

(83)   Shkrob, I. A.; Zhu, Y.; Marin, T. W.; Abraham, D. *J. Phys. Chem. C* **2013**, 130913123008003.

(84)   Ota, H.; Akai, T.; Namita, H.; Yamaguchi, S.; Nomura, M. *J. Power Sources* **2003**, *119-121*, 567.

(85)   El Ouatani, L.; Dedryvère, R.; Siret, C.; Biensan, P.; Gonbeau, D. *J. Electrochem. Soc.* **2009**, *156* (6), A468.

(86)   Ding, L.; Li, Y.; Li, Y.; Liang, Y.; Huang, J. *Eur. Polym. J.* **2001**, *37*, 2453.

(87)   Parks, G. S.; Mosher, H. P. *J. Polym. Sci. Part A* **1963**, *1*, 1979.

(88)   Ding, L.; Hennig, I.; Evsyukov, S. E. *Polymer* **2001**, *42* (7).

(89)   Xiong, D.; Burns, J. C.; Smith, A. J.; Sinha, N.; Dahn, J. R. *J. Electrochem. Soc.* **2011**, *158* (12), A1431.

(90)   Takamatsu, D.; Orikasa, Y.; Mori, S.; Nakatsutsumi, T.; Yamamoto, K.; Koyama, Y.; Minato, T.; Hirano, T.; Tanida, H.; Arai, H.; Uchimoto, Y.; Ogumi, Z. *J. Phys. Chem. C* **2015**, *119* (18), 9791.

(91)   Kim, T.; Assary, R. S.; Pauls, R. E.; Marshall, C. L.; Curtiss, L. A.; Stair, P. C. *Catal. Commun.* **2014**, *46*, 66.

(92)   Aurbach, D.; Gamolsky, K.; Markovsky, B.; Gofer, Y.; Schmidt, M.; Heider, U. *Electrochimica Acta* **2002**, *47* (9), 1423.

(93)   Ma, L.; Self, J.; Nie, M.; Glazier, S.; Wang, D. Y.; Dahn, J. R. *Submitted to J. Power Sources* **2015**.

(94)   Xia, J.; Self, J.; Ma, L.; Dahn, J. R. *J. Electrochem. Soc.* **2015**, *162* (8), A1424.

(95)   Becke, A. D. *Phys. Rev. A* **1988**, *38* (6), 3098.

(96)   Wodrich, M. D.; Corminboeuf, C.; Schreiner, P. R.; Fokin, A. A.; Schleyer, P. von R. *Org. Lett.* **2007**, *9* (10), 1851.

(97)   Wang, R. L.; Dahn, J. R. *J. Electrochem. Soc.* **2006**, *153* (10), A1922.

(98)   Wang, Y.; Xing, L.; Tang, X.; Li, X.; Li, W.; Li, B.; Huang, W.; Zhou, H.; Li, X. *RSC Adv.* **2014**, *4* (63), 33301.

(99)   Zhang, Z.; Hu, L.; Wu, H.; Weng, W.; Koh, M.; Redfern, P. C.; Curtiss, L. A.; Amine, K. *Energy Environ. Sci.* **2013**, *6* (6), 1806.

(100)   Tomasi, J.; Mennucci, B.; Cammi, R. *Chem. Rev.* **2005**, *105* (8), 2999.

(101)   Tomasi, J.; Mennucci, B.; Cancès, E. *J. Mol. Struct. THEOCHEM* **1999**, *464* (1–3), 211.

(102)   Conway, B. E. *Theory and principles of electrode processes*; Modern concepts in chemistry; New York, Ronald Press Co1965, 1965.

(103)   Weng, W.; Zhang, Z.; Redfern, P. C.; Curtiss, L. A.; Amine, K. *J. Power Sources* **2011**, *196* (3), 1530.

(104)   Li, Z. D.; Zhang, Y. C.; Xiang, H. F.; Ma, X. H.; Yuan, Q. F.; Wang, Q. S.; Chen, C. H. *J. Power Sources* **2013**, *240*, 471.

(105)   Vollmer, J. M.; Curtiss, L. A.; Vissers, D. R.; Amine, K. *J. Electrochem. Soc.* **2004**, *151* (1), A178.

(106)   Isse, A. A.; Gennaro, A. *J. Phys. Chem. B* **2010**, *114* (23), 7894.

(107) Vaný́sek, P. In *CRC Handbook of Chemistry and Physics (Internet Version 2015)*; CRC Press/Taylor and Francis: Boca Raton, Florida, USA, 2015.

(108) Asselin, E.; Alfantazi, A.; Rogak, S. *Corrosion* **2008**, *64* (4), 301.

(109) Pourbaix, M. In *Atlas d'Équilibres Électrochimiques à 25 °C*; Gauthier-Villars & Cie: Paris, France, 1963; pp 330–342.

(110) Hall, D. S.; Lockwood, D. J.; Bock, C.; MacDougall, B. R. *Proc. R. Soc. A* **2015**, *471* (2174), 20140792.

(111) Oliva, P.; Leonardi, J.; Laurent, J. F.; Delmas, C.; Braconnier, J. J.; Figlarz, M.; Fievet, F.; Guibert, A. de. *J. Power Sources* **1982**, *8* (2), 229.

(112) Dahn, H. M.; Smith, A. J.; Burns, J. C.; Stevens, D. A.; Dahn, J. R. *J. Electrochem. Soc.* **2012**, *159* (9), A1405.

(113) Shirley, D. A. *Phys. Rev. B* **1972**, *5* (12), 4709.